PROTON INDUCED K X-RAY FLUORESCENCE AS AN ANALYTICAL TOOL

by

CLAUDE LAPOINTE

A THESIS

Submitted to the Faculty of Graduate Studies in Partial Fulfillment of the Requirements for the Degree

MASTER OF SCIENCE

Department of Physics
University of Manitoba
Winnipeg, Manitoba

PROTON INDUCED K X-RAY FLUORESCENCE AS AN ANALYTICAL TOOL

BY

JOSEPH ROBERT CLAUDE LAPOINTE

A thesis submitted to the Faculty of Graduate Studies of the University of Manitoba in partial fulfillment of the requirements of the degree of

MASTER OF SCIENCE

ABSTRACT

The work described in this thesis was undertaken from September 1978 to September 1980 at the University of Manitoba Cyclotron Laboratory. Two separate projects which are related to Proton Induced X-ray Emission (PIXE) are reported in the second and third chapters. The first chapter summarizes the fundamentals of characteristic X-ray emission as a means of elemental identification.

The second chapter details an entirely new probe composed of a number of horizontal strips of different elemental composition which is used to deduce the intensity distribution and position H^- beam inside the University of Manitoba Cyclotron. The principles behind the operation of the probe are basically simple. H^- ions are accelerated within the cyclotron and strike the probe where they induce X-ray emission. Identification of the characteristic X-rays indicates what portion of the probe was struck. A Fortran computer program was written to estimate the intensity of the current on each strip from the intensity of the characteristic X-rays. The advantages of this new analytical tool have already been published (La80).

The third chapter describes how the PIXE technique has been used at the University of Manitoba to accurately measure the concentration of cesium in brain of mice treated daily with an intraperitoneal injection of cesium chloride (CsCl). These studies were started by Dr. C. Pinsky of the Department of Pharmacology and Therapeutics of the

Faculty of Medicine at the University of Manitoba to anticipate the possible biohazards of cesium ions. The technique used employs an internal standard, namely dysprosium, added in a precisely known amount to the brain sample. The relative intensity of the cesium and dysprosium peaks is then used as a means of estimating the concentration of cesium in mouse brain.

ACKNOWLEDGEMENTS

I wish to acknowledge the assistance of Dr. J.S.C. McKee who proposed the projects described in this thesis and supervised my work. I wish to thank Dr. S. Standil for assistance provided to me in the early stage of my work. Thanks are also due to Dr. Jim Birchall for his unfailing collaboration. I am grateful to all the cyclotron staff and in particular the members of the so-called "PIXE Group" for their helpfulness. Finally, I would also like to thank Dr. C. Pinsky and Dr. R. Bose, from the Health Science Center, for providing us with the mouse brain sample targets used in PIXE studies.

TABLE OF CONTENTS

ABSTRACT ii

ACKNOWLEDGEMENTS iv

TABLE OF CONTENTS v

LIST OF FIGURES vii

LIST OF TABLES ix

CHAPTER 1. FUNDAMENTALS OF X-RAY FLUORESCENCE

1.1 INTRODUCTION 2

1.2 CHARACTERISTIC X-RAYS 3

1.3 X-RAY FLUORESCENCE INSTRUMENTATION 6

1.3.1 The semiconductor detector

1.3.2 The preamplifier and main amplifier

1.3.3 The multi-channel analyser

1.3.4 Data processing

1.3.5 Excitation system

CHAPTER 2. A K X-RAY FLUORESCENT MULTI-STRIP PROBE FOR ACCELERATOR BEAM STUDIES

2.1 INTRODUCTION 11

2.2 THE MULTI-STRIP PROBE 13

2.2.1 Principles of the probe

2.2.2 Selection of metals for the probe

2.3 CALCULATION OF BEAM INTENSITY DISTRIBUTION 25

2.3.1 The program 'PROBE'

2.3.2 Results of computation

2.3.3 Accuracy of calculation

2.4 DETECTION LIMIT 39

2.5 EXPERIMENTAL CHECK OF THE PROGRAM 40

2.6 RESULTS OF MEASUREMENT AND CONCLUSION 43

CHAPTER 3. ANALYSIS OF CESIUM IN MOUSE BRAIN SAMPLES USING THE PIXE TECHNIQUE

3.1 INTRODUCTION 46

3.2 TECHNIQUE OF MEASURING CESIUM CONCENTRATION IN SAMPLES 48

3.2.1 Preparation of target samples

3.2.2 Experimental technique and theoretical estimation

3.2.3 Correction for attenuation and detector efficiency

3.2.4 Concentration of cesium in brain samples

3.3 CONCLUSION 62

3.4 FUTURE WORK 63

REFERENCES 66

LIST OF PUBLICATIONS 68

LIST OF FIGURES

FIGURE		PAGE
1.1	Schematic of atomic levels	4
2.1	Schematic of the multi-strip probe	14
2.2	Diagram of experimental set-up in multi-strip probe experiment	16
2.3	Meaning of the parameters used in the derivation of the thick target equation	17
2.4	Spectra of bremsstrahlung obtained with R.F. voltage of 24 and 28 kV	20
2.5	A plot of K shell ionization cross-sections in barns vs the proton energy in MeV for different elements	23
2.6	A plot of the number of K X-rays detected per μC of charge vs the position of the probe inside the cyclotron for a set of metals	30
2.7	Typical spectrum obtained with the multi-strip probe ...	32
2.8	A plot of the total number of Sn K_α X-rays emitted as a function of depth in target for different incident energies of incident protons	36
2.9	Vertical distribution of the beam current at different radii inside the cyclotron as deduced using the multi-strip probe	44
3.1	Floor plan of the University of Manitoba Cyclotron showing the location of the "PIXE cube" on "C" line	50

3.2 Diagram of experimental set-up used in PIXE experiment 51

3.3 Typical X-ray spectrum of mouse brain sample 52

LIST OF TABLES

TABLE		PAGE
2.1	X-ray transmission through the aluminum exit window at different X-ray energies	22
2.2	Coefficients C_{mn} for the calculation of the stopping power using equations (4) and (5)	27
2.3	Coefficients B_n for the calculation of K shell ionization cross-sections	29
2.4	Area of the peaks observed in the spectrum obtained with the probe positioned at a radius of 9"	33
2.5	Current (in nA) on the metal strips struck by the proton beam with probe positioned at a radius of 9" ...	35
2.6	Comparison between the number of characteristic X-rays detected per μC of charge incident on a thick erbium target as measured experimentally and as calculated using the program "PROBE"	42
3.1	K X-ray production cross-section of cesium and dysprosium for an energy of the incident protons of 30 MeV	54
3.2	Transmission of K X-rays of cesium and dysprosium through 2 cm of paraffin	57
3.3	Comparison between the calculated values of transmission for γ-rays and X-rays of Am-241 through the paraffin absorber and the experimentally measured values	59

CHAPTER 1

FUNDAMENTALS OF X-RAY FLUORESCENCE

1.1 INTRODUCTION

The value of X-ray energy spectroscopy (XES) is now well established, as evidenced by the widespread use and number of different types of instruments that have been formulated for the application of this technique. X-ray fluorescence (XRF) and proton induced X-ray emission (PIXE) studies applied to identification of elemental composition of materials, have attracted a great deal of interest in recent years. The advantages of those analytical techniques are:

- Element identification via the characteristic x-ray spectra is simplified due to the relative simplicity of the x-ray spectra.
- X-ray analysis is non destructive, the inspection by radiation taking place without altering the composition of the specimen. It is then preserved for possible re-examination by the same or other analytical techniques.
- An analysis of the characteristics X-rays results in a spectrum containing several peaks that may be easily interpreted in both a qualitative and quantitative sense.
- Opportunity to scan a large proportion of the periodic table of the elements in a single measurement.
- The high detection efficiency and high energy resolution of the semiconductor detector (Si(Li), Ge(Li) or hyperpure germanium).

Since the basis of XES has been amply covered in the literature (Be70), only a brief summary of the fundamentals will be presented here.

1.2 CHARACTERISTIC X-RAYS

To describe the foundation of X-ray emission as a means of element analysis, it shall be sufficient to use the simplified image of the atom as a spherical structure, see Figure 1.1. Each shell (labeled K, L, M, N etc starting with the innermost one) is characterized by a definite value of the "binding energy" of the electrons in the shell. This is the minimum energy required to free an electron from its binding to the nucleus. Most importantly, this characteristic binding energy of a given shell is closely related to the charge of the nucleus which effectively characterizes the atomic element (i.e. its atomic number).

The above description is oversimplified, in that it is found that the major levels are split into a number of sub-levels, as shown in Figure 1.1. However, this does not change the basic properties as outlined above.

X-ray fluorescence, or the generation of X-ray radiation from an atom, is achieved through any interaction that excites or removes an electron from its normal place in the atom. The atom will subsequently seek to revert back to its original electronic configuration. This takes place when electrons from some higher shell are transferred to the vacant electron site. Such electron transitions imply a loss of energy and the requirement of energy conservation is satisfied by the emission of electromagnetic radiation (X-ray) carrying an amount of energy equivalent to the energy difference between the two shells of the electron transition. Due to the discrete energy values of the permissibles

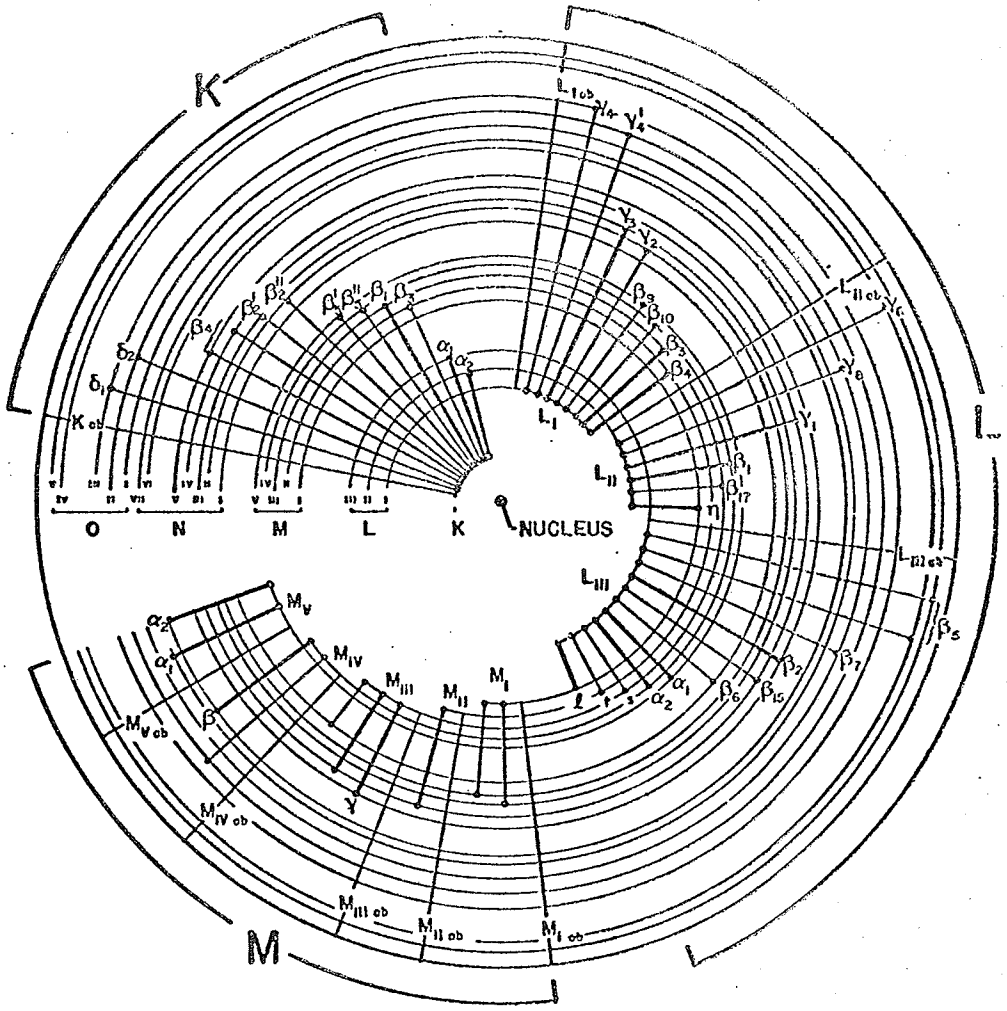

Fig 1.1 Atomic shell model, showing electron transitions that may follow electron vacancies (Wo73).

shells, there will be a well defined set of energies associated with the emitted X-rays. Since the energy values of the shells are characteristic of the atomic element, the emitted X-rays will always be characteristic of the element from which it originates. It is worth mentioning that by virtue of their involving tightly bound inner shell electron, the energy levels, and therefore the energies of the emitted X-rays, are essentially insensitive to the chemical environment.

It should also be mentioned that an electronic vacancy does not always lead to the emission of an X-ray. Although no X-ray emission takes place, the effect may be visualized as the reabsorption of the characteristic X-ray by an electron from higher shells in the same atom. This electron, known as an Auger electron, is then ejected, and the original X-ray is "lost". This competitive effect to characteristic X-ray emission introduces a factor called the fluorescent yield, which is defined as the ratio of emitted X-rays to the number of primary vacancies created.

1.3 X-RAY FLUORESCENCE INSTRUMENTATION

1.3.1 The semiconductor detector

To determine the presence of a chemical element, of course, the emitted radiation must be detected. This is usually performed by semiconductor detectors which combine high detection efficiency and high resolution. High resolution lies at the very heart of the operation since characteristic X-rays of neighbouring elements in the periodic table can be very close in energy.

To establish the qualitative and quantitative presence of two or more elements, the system must be able to measure the energy of the characteristic X-rays. The semiconductor detector detects and distinquishes the presence of chemical elements on an intrinsic energy basis. A very important consequence of this detection mode is that analysis for all chemical elements is performed simultaneously.

The principle behind the semiconductor detector is relatively simple. By definition, a semiconductor is a material that is very poor conductor of electric current. Hence, very little current will flow through the crystal when an electric potential is applied to it. The absorption, by the crystal, of ionizing radiation (as X-ray) creates an amount of "free" charge which is swept out by the applied voltage as a charge pulse. However, the electrical noise arising from thermally-generated free charge at room temperature will swamp the radiation-induced charge. Hence the crystal is cooled to the temperature of liquid nitrogen in order to obtain the desired detection performance

characteristic. The high capability of the semiconductor to distinguish the X-ray energy rests on the linearity between the electric charge created and the energy of the X-ray. This is constrained, of course, by the physical requirement that the X-ray loses all its energy during interaction with the crystal.

1.3.2 The preamplifier and main amplifier

The absorbed X-ray is presented as a burst of charge collected at the detector terminal. The first stage of the preamplifier employs a field-effect transistor (FET) built into the system in very close proximity to the detector and also cooled to the temperature of liquid nitrogen in order to keep the electronic noise to a minimum. The function of the preamplifier is to integrate the total charge of the pulse and convert it to a voltage signal retaining the proportionality to the energy deposited.

The fundamental function of the main amplifier is to amplify the signals from the preamplifier and condition the signal for sorting and recording according to pulse height.

1.3.3 The multi-channel analyser

The full utilisation of the capability of the semiconductor detector system is realized by means of the multi-channel analyser (MCA). Fundamentally, the MCA counts and stores the pulses presented from the amplifier according to their height. The MCA produces an "intensity

vs energy" distribution of the detected X-rays, which may be displayed in analog form on an oscilloscope monitor, or be plotted out on an X-Y plotter.

1.3.4 Data processing

The "raw" spectrum produced by the MCA may at times be sufficient to complete the analysis. More often, various steps of processing the raw data are necessary in order to extract such quantitative information as:

- The determination of the energy of the X-rays corresponding to the "peaks" in the recorded spectrum. This establishing of the energy scale is called the energy calibration of the system which requires the identification of the position of at least two peaks of known energy.
- Determination of the intensity of the characteristic X-ray emission by integrating the area of the peak. This incorporates some means of identifying and subtracting the background underlying the peak.
- Explicit element identification by comparison of spectrum peak energies with a listing of characteristic X-ray energies for the element.

1.3.5 Excitation system

As mentioned earlier, the production of X-ray radiation from

an atom is achieved through any interaction that removes an electron from its normal place in the atom. In the practical application of XES analysis, two different approaches are employed, i.e., fluorescence by means of a primary source of electromagnetic radiation (X-ray tubes, X-rays and γ-rays from radioactive sources), or by means of charged particle beams (e.g. electrons, protons, alpha particles).

CHAPTER 2

A K X-RAY FLUORESCENT MULTI-STRIP PROBE FOR ACCELERATOR BEAM STUDIES

2.1 INTRODUCTION

Particles in a cyclotron can travel a significant distance before reaching their final energy. In the case of the University of Manitoba facility the distance will lie between 0.5 and 2 kilometers. The Cyclotron magnetic field influences particles in such a way that particles which depart from an isochronous orbit will oscillate back and forth about the mean trajectory, not only sideways but also in the vertical plane. These oscillations are called radial and axial betatron oscillations, respectively.

It is always useful, and on occasions essential, to be able to measure accurately the position of a particle beam within an accelerator and, in addition, the intensity distribution of the particles in the beam. These measurements became particularly important at the University of Manitoba Cyclotron when polarised ions were accelerated.

A particle located exactly in the median plane of the machine is subject only to a vertical magnetic field. Due to the particular shape of the magnetic field inside the machine, a particle out of the median plane will experience an oscillating horizontal field. When the frequency of the horizontal field component varies as the particle is accelerated, the particle can be in resonance with its spin precession frequency around the vertical component of the cyclotron field. This process can cause a net re-orientation of the particle spin during passage through this resonance region resulting in a depolarisation effect on the beam (for more details see (Oh79)).

The traditional method by which the ion beam is viewed directly

on a ZnS or other fluorescent screen is often useful in determining the vertical position of the beam, but yields little information about the relative intensities within the beam spot. For this reason it was decided to design an entirely new probe which would take advantage of the unique features of the K-shell fluorescence study of medium and heavy elements. These features are:

a) High yields for proton beams above 10 MeV incident energy.

b) Clean identification of all intermediate and heavy elements through K X-ray measurement, using an Ortec hyperpure germanium detector (Model 1113-10205) with a resolution better than 0.4% at 120 keV and high efficiency throughout this elemental range.

c) Small self absorption of K X-rays in the probe as compared with the much lower energy L X-rays from the same element.

2.2 THE MULTI-STRIP PROBE

2.2.1 Principles of the probe

The probe consists of a set of metal strips of pure elemental composition, covering a wide range of atomic numbers. The strips are approximately 1 cm long, 2 mm wide and about 0.1 mm thick. They are mounted horizontally on the end face of an adjustable radial probe so as to form a vertical multi-component foil, as shown in Figure 2.1. The twelve elements chosen on the basis of suitability and availability were, from bottom to top (see Fig. 2.1): tin, gold, erbium, lead, platinum, samarium, ytterbium, tantalum, indium, gadolinium, holmium and rhenium (later calculations and experiments showed that some of those elements, namely, gold, platinum and lead were in fact not appropriate because the K shell ionization cross-section is small for these elements and leads to a poor sensitivity). The probe and foil could be accurately positioned at any required radius within the cyclotron by means of a remote control system.

The principles behind the operation of the probe and the interpretation of the measurements made with it are basically simple. Negative H^- (or protons) are accelerated within the four sector cyclotron and strike the probe where they induce K shell ionization. The vacancies created are quickly followed by K X-ray emission. The characteristic K X-rays are detected by means of an Ortec hyperpure germanium detector (Model 1113-10205). The pulses from the detector are amplified using an Ortec Spectroscopy Amplifier (Model 472A) and energy spectra are

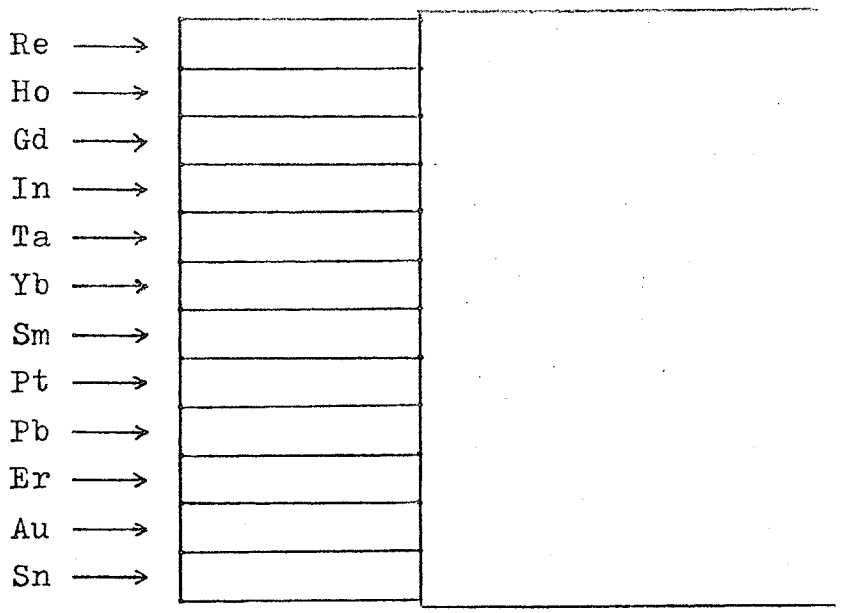

Fig. 2.1 Schematic of the multi-strip probe.

collected by an on-line PDP 15/20 computer using the data collection program MIRAD. The spectra are recorded in 1024 channels and stored on DEC tapes for later off-line analysis (see Figure 2.2). The characteristic K X-rays detected indicate that at least some portion of the beam has struck a particular elemental strip of the foil. The intensity I_p (in μA) of the proton beam striking a particular strip can be expressed by the equation:

$$I_p = \frac{I_k(\alpha,\beta)}{N(\alpha,\beta)} \qquad \text{Eq. (1)}$$

where $N(\alpha,\beta)$ is the number of characteristic K_α (or K_β) X-rays that would be detected per second for an incident current of 1 μA and $I_K(\alpha,\beta)$ is the number of K_α (or K_β) X-rays effectively detected. $N(\alpha,\beta)$ can be deduced in the same way as indicated by reference (De75) from the equation:

$$N(\alpha,\beta) = \frac{\rho N \Omega}{A} W_K F(\alpha,\beta)\, \varepsilon(\alpha,\beta)\, e^{-\mu' t'} \int_0^{T'} \sigma_K(E) \exp\left(-t\mu\rho \frac{\cos\theta_i}{\cos\theta_d}\right) dt \qquad \text{Eq. (2)}$$

where the parameters used in the above formula are as follow (see Figure 2.3).

I_p: the number of incident protons per unit time (intensity of the beam) on a given metal strip.

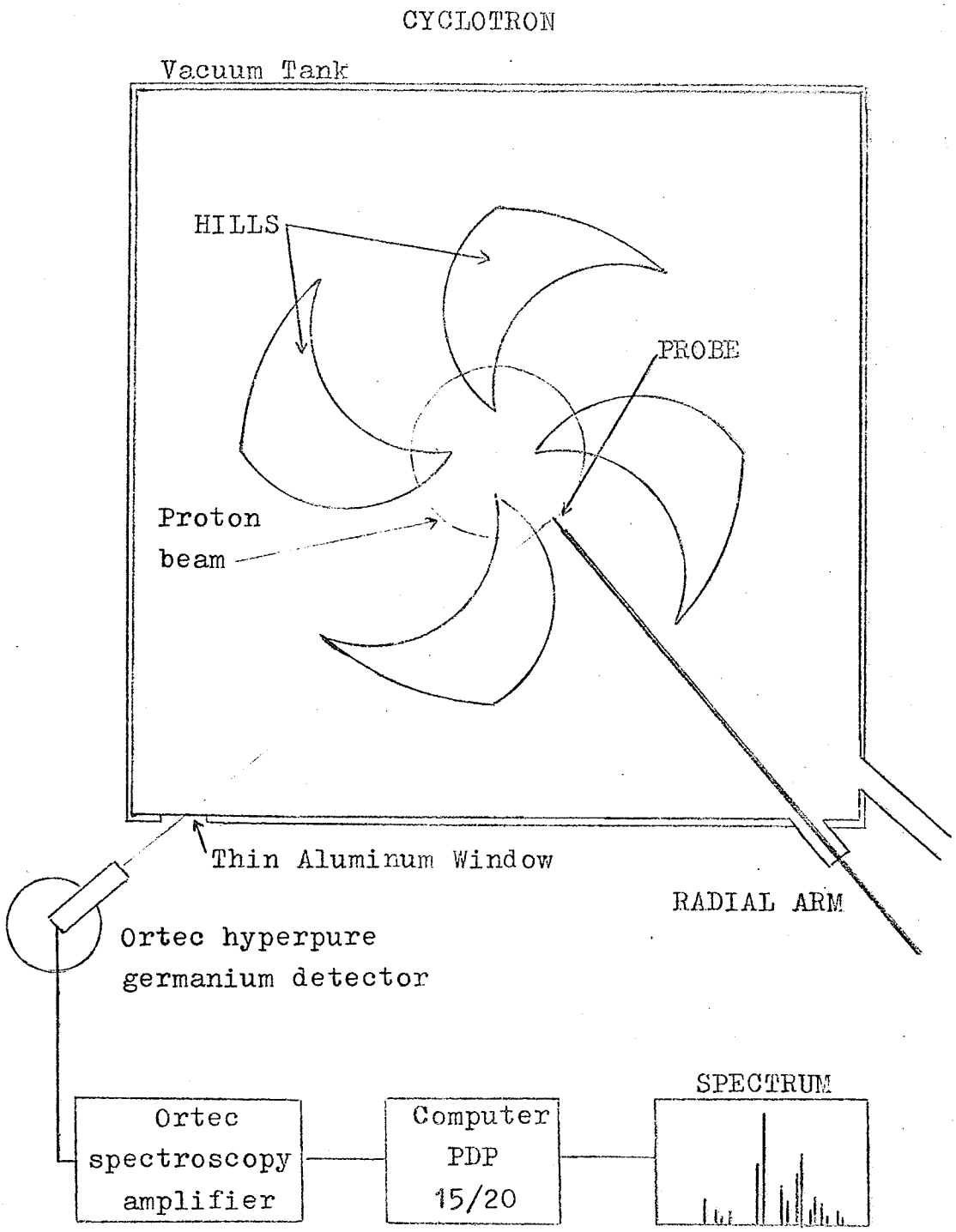

Fig. 2.2 Diagram of experimental set-up showing the location of multi-strip probe inside the cyclotron vacuum tank.

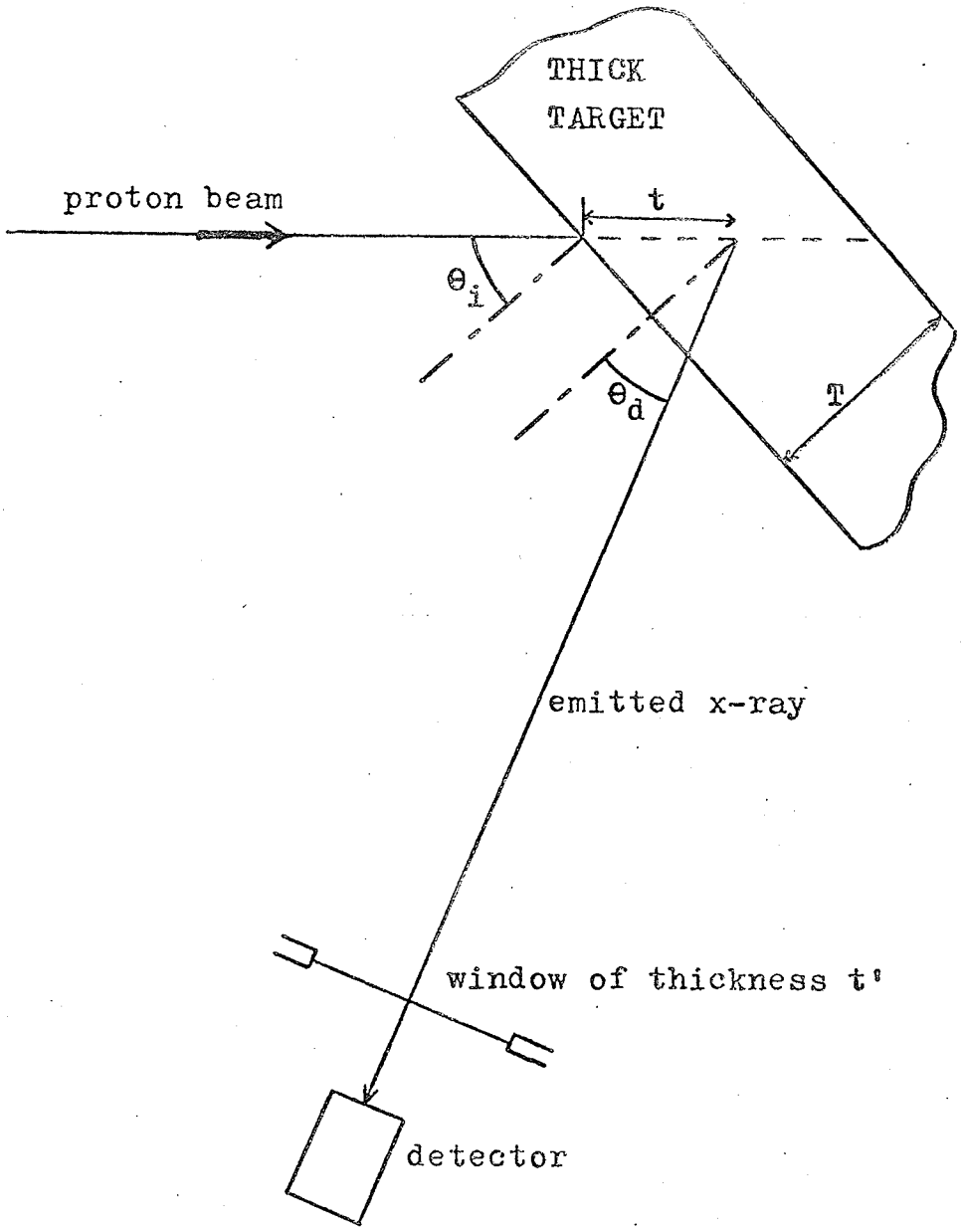

Fig. 2.3 Meaning of the parameters used in the derivation of thick target equation.

ρ : the density of metal

N : Avogadro's number

A : the atomic weight of the element under consideration

Ω : the solid angle subtended by the detector

W_K : the fluorescence yield for K shell ionisation

$F(\alpha,\beta)$: the proportion of K_α (or K_β) X-rays emitted compared to the total number of K X-rays emitted

$\varepsilon(\alpha,\beta)$: the efficiency of the detector for K_α (or K_β)

$\mu'(\alpha,\beta)$: mass absorption coefficient of K_α (or K_β) X-rays in aluminum

t' : the effective thickness of the exit window

$\exp(-\mu' t')$: the attenuation of K_α (or K_β) X-rays within the exit window

T' : the apparent thickness of the strip ($T/\cos\theta_i$ where T is the target thickness and θ_i the angle of incidence of the proton beam)

$\sigma_K(E)$: K-shell ionisation cross-section (function of proton energy)

μ : the mass absorption coefficient in target (self-absorption)

θ_i : the angle of incidence of the proton beam

θ_d : the detector angle

$\exp(-t\rho\mu \cos\theta_i/\cos\theta_d)$: attenuation of outgoing K_α (or K_β) X-rays in the target (function of the depth t)

with

$$E(t) = E_o - \int_o^t \Delta E \, dt \qquad \text{Eq. (3)}$$

where E(t) is the energy of the protons at a given depth t in target, ΔE the energy loss per unit length (stopping power of the target material) which is a function of energy E(t) and E_o the energy of the incident protons.

The term $N(\alpha,\beta)$ is calculated numerically, and $I_K(\alpha,\beta)$ is the result of the experimental measurement. I_p, the intensity of the beam striking the particular strip, can be deduced from these two quantities.

2.2.2 Selection of metals for the probe

The choice of the best metals to be used in making the probe is limited by the sensitivity allowed by a given metal which determines the value of the minimum current striking the strip and still measurable. This sensitivity depends mainly upon the energy of the characteristic K X-rays and the K shell ionization cross-section.

The first restriction on the sensitivity is due to the bremsstrahlung radiation produced by electrons coming from residual gas molecules that are accelerated by the R.F. voltage and stopped into the dees. The end-point of the bremsstrahlung background could be varied by adjustment of the R.F. voltage as can be seen in Figure 2.4 which shows two bremsstrahlung spectra obtained with R.F. voltages of 24 and 28 kV. This bremmstrahlung radiation starts at 28 keV (for R.F. voltage of 28 kV which is used at the U of M cyclotron) and increases very quickly below 20 keV. This very high background at low energy was responsible for a high dead time in the detector electronics which seriously interferes with normal counting. This forced us to replace the Kapton (*)

(*) Polyimide film, Registered TM DUPONT.

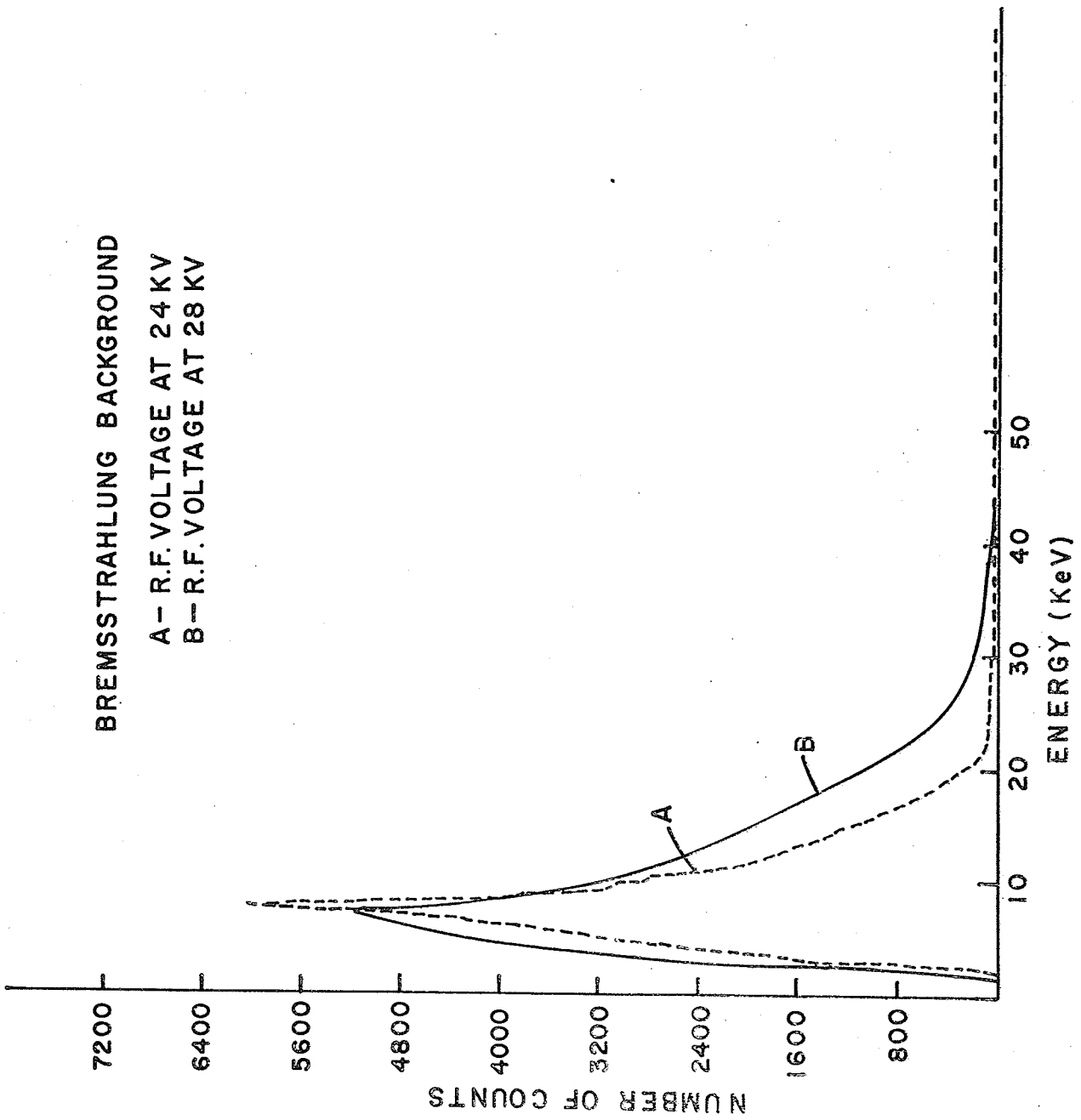

Fig 2.4 Spectra of Bremsstrahlung background obtained with R.F. voltage of 24 and 28 kV.

viewing window on the cyclotron vacuum tank by a thin aluminum window (50 mils thick) which stops most of the low energy X-rays. Table 2.1 gives the transmission through the exit window for different X-ray energies; the thickness of the window used for the calculation was 75 mils since, in the configuration of the experimental set up, the outgoing X-rays must go through the window with an incident angle of about 45 degrees. The table shows that if the transmission through the exit window is still 17% for a X-ray energy of 20 keV, it is less than 2% at 15 keV and decreasing very quickly. This obviously prohibited the use of metals with low-energy characteristic K X-rays.

Another restriction comes from the relatively low K shell ionization cross-section for heavy elements at a given proton energy with respect to the ionization cross-section of lighter elements at the same proton energy. Figure 2.5 shows a plot of the ionization cross-section (in barns) versus the energy of the incident proton (in MeV) for different values of atomic numbers. It can be seen from the plot that the K shell ionization cross-section varies by several orders of magnitude over the periodic table of elements (especially at proton energies of a few MeV). The use of heavy elements, for which the ionization cross-section is small, in the probe would then force us to wait a much longer time in order to obtain good statistics in the characteristic X-ray peaks. Heavy elements like lead, gold and platinum should not be used. In the case of lead, its low melting point (327 C) makes it even less recommendable. (During the preliminary experiments made with the probe, the heat produced by the proton beam whose power could reach 1 watt, melted down the lead strip ...)

In order to calculate the beam intensity hitting a particular

TABLE 2.1

X-ray transmission through the aluminum window (0.075" (0.19 cm) effective thickness) for different X-ray energies. Mass absorption coefficients are from (Ve73).

X-ray Energy (keV)	Mass abs. coefficient of Al (cm^2/g)	Transmission
10	26.1	$1.48 \cdot 10^{-6}$
15	7.92	0.017
20	3.41	0.173
30	1.12	0.562
40	0.567	0.747
50	0.368	0.827
60	0.279	0.866
80	0.202	0.901

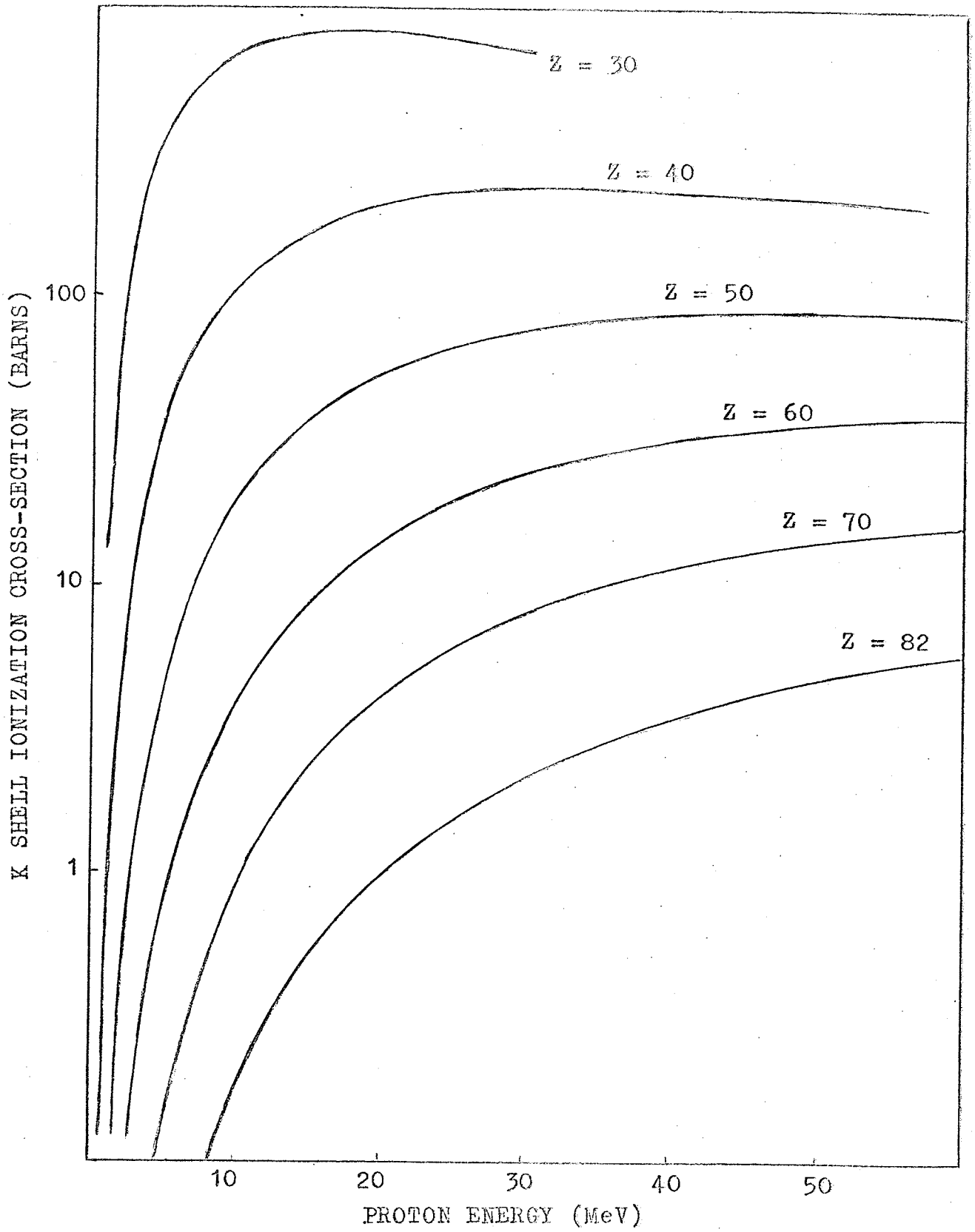

Fig. 2.5 A plot of K shell ionization cross-sections vs proton energy for different elements.

strip, a computer program (code name PROBE) was written. It solves numerically equation (2) for any element and any energy of the incident proton (between 2 MeV and 1.2 GeV). The output was defined so as to give the number of characteristic K X-rays effectively detected per second for an assumed incident current of 1 μA on a given strip. The rate of K X-rays effectively detected during a measurement (corrected for the dead time of the detector) divided by the number predicted for an incident current of 1 μA gives immediately the incident current in μA.

Since the whole purpose of the probe is to measure the intensity distribution within the beam spot, the width of the strips is very important since it determines the "resolution power" of the probe. The narrower are the strips the better will be the resolution. During the measurement, it appeared that the beam spot can be as small as 6 mm in diameter and consequently each strip could be no more than 2 mm wide in order to give, at least, a rough idea of the intensity distribution within the beam (the beam spot being then "cut" into 3 or 4 "slices"). The total width of the probe is also important since, if the amplitude of oscillation becomes too great, some part of the beam may not strike the probe. It appeared that a total width of 25 mm was sufficient to follow any oscillation. Beside that, a width of 25 mm is the maximum that can be fitted on the end of a radial probe for insertion into the machine. The use of a bigger probe would necessitate venting of the machine and the removal of the radial arm mechanism from the vacuum tank so to be able to attach the probe to the arm.

2.3 CALCULATION OF BEAM INTENSITY DISTRIBUTION

2.3.1 The program 'PROBE'

The program PROBE solves equation (2) numerically. The integral part of the equation is replaced by a sum. The size of the steps in the sum was defined so that a further reduction in it does not introduce any significant change in the numerical results.

From equation (2), it can be seen that it is necessary to provide for every element of interest a series of 13 parameters (density, atomic number, atomic mass, mass absorption coefficients ...). To avoid repeating the entry of these numbers for every calculation, they were stored on disc where they were readily available to the computer whenever needed. The calculation also requires the value of K shell ionization cross-section $\sigma_K(E)$ which requires the knowledge of the proton energy at every point in the target. The energy can then be calculated if we know the energy loss per unit length ΔE (stopping power) of the material which is also a function of the proton energy. It quickly appeared a lot more conver ient to have an analytical representation for the stopping power for the range of energy which precludes the necessity of having to rely on a large table of numbers.

Barkas and Berger (Ba64) have made a search for an optimum formula and have found it convenient to represent the proton stopping power by the following expression:

$$\frac{dE}{dR} = \frac{E}{R} \left\{ \sum_n \sum_m n A_{nm} (\log I)^m (\log E)^{n-1} \right\}^{-1} \qquad \text{Eq. (4)}$$

with

$$R = \frac{A}{Z} \exp\left\{ \sum_n \sum_m A_{nm} (\log I)^m (\log E)^n \right\} \qquad \text{Eq. (5)}$$

where dE/dR is the energy loss in MeV/g-cm^2, E is the kinetic energy of protons, R the proton range in g-cm^2 (note that equation (5) was first obtained by Barkas and Berger by fitting experimental values of ranges as a function of proton energy. Equation (4) is then obtained from equation (5) by differentiation). A is the atomic mass, Z the atomic number. I is the mean excitation energy of the medium which can be expressed by the semi-empirical formula (Ba64)

$$I = 9.76\ Z + 58.8\ Z^{-0.19} \quad \text{eV} \qquad \text{Eq. (6)}$$

$$\text{for } Z > 12$$

and the coefficient A_{nm} obtained by least-squares adjustment of the data are given in Table 2.2.

The ionization cross-section $\sigma_K(E)$ was defined analytically from the semi empirical formula of Johansson and Johansson (Jo76) based on thin target measurements. The ionization cross-section (in barns) is given by

$$\sigma_K = 10^{10} \exp\left(\sum_n B_n x^n \right) \qquad \text{Eq. (7)}$$

where

$$x = \log (E/r\ u) \qquad \text{Eq. (8)}$$

TABLE 2.2

Coefficients C_{mn} in equations (4) and (5) for proton energy ranging from 1 MeV to 8 MeV.

m \ n	0	1	2
0	$-7.5265 \cdot 10^{-1}$	2.5398	$-2.4598 \cdot 10^{-1}$
1	$7.3736 \cdot 10^{-2}$	$-3.1200 \cdot 10^{-1}$	$1.1548 \cdot 10^{-1}$
2	$4.0556 \cdot 10^{-2}$	$1.8664 \cdot 10^{-2}$	$-9.9661 \cdot 10^{-3}$

Coefficients C_{mn} for proton energy ranging from 8 MeV to 1.2 GeV (*).

m \ n	0	1	2	3
0	-8.0155	1.8371	$4.5233 \cdot 10^{-2}$	$-5.9898 \cdot 10^{-3}$
1	$3.6916 \cdot 10^{-1}$	$-1.4520 \cdot 10^{-2}$	$-9.5873 \cdot 10^{-4}$	$-5.2315 \cdot 10^{-4}$
2	$-1.4307 \cdot 10^{-2}$	$-3.0142 \cdot 10^{-2}$	$7.1303 \cdot 10^{-3}$	$-3.3802 \cdot 10^{-4}$
3	$3.4718 \cdot 10^{-3}$	$2.3603 \cdot 10^{-3}$	$-6.8538 \cdot 10^{-4}$	$3.9405 \cdot 10^{-5}$

(*) Using this second set of coefficients, the stopping power obtained from equation (4) is in MeV/mg-cm^2 instead of MeV/g-cm^2.

where u is the ionization energy, E the proton energy (both in eV) and r is the ratio of the proton mass to the electron mass (r = 1840). The values of the coefficients B_n are given in Table 2.3.

2.3.2 Results of computation

The calculations using the program PROBE were performed on a PDP15/40 computer at the University of Manitoba Cyclotron Laboratory. Calculations were made for a set of metals covering the range from zinc (Z = 30) to lead (Z = 82), and for different radii (distance to center of cyclotron) from 3 inches up to 10 inches by intervals of 0.5 inch. For sake of clarity only part of the results are shown in Figure 2.6. The results are presented as the number of K_α X-rays that would be detected per second for an incident current of 1 μA.

One can see from Figure 2.6 that metals with atomic numbers, Z, greater than 50 have a decreasing sensitivity due to their decreasing K shell ionization cross-section. In order to keep a reasonable sensitivity, one should not use any metal with a Z value higher than 68 (it will be seen why the value Z = 68 was chosen). The sensitivity reaches its maximum for metals having values of Z in the range 40 to 50. The element with the smallest value of Z and still appropriate is yttrium (Z = 39). Below Z = 39, there is a series of elements which are not available in metallic form and below that series the K X-ray energies are too small and the attenuation in the exit window becomes too important. One should also mention that silver (Z = 43) can not be used at the University of Manitoba Cyclotron since

TABLE 2.3

Coefficients B_n for the calculation of K shell ionization cross-sections using equation (7).

$B_o = 2.0471$	$B_3 = 9.9190 \cdot 10^{-2}$
$B_1 = -6.5906 \cdot 10^{-3}$	$B_4 = 4.6063 \cdot 10^{-2}$
$B_2 = -4.7448 \cdot 10^{-1}$	$B_5 = 6.0853 \cdot 10^{-3}$

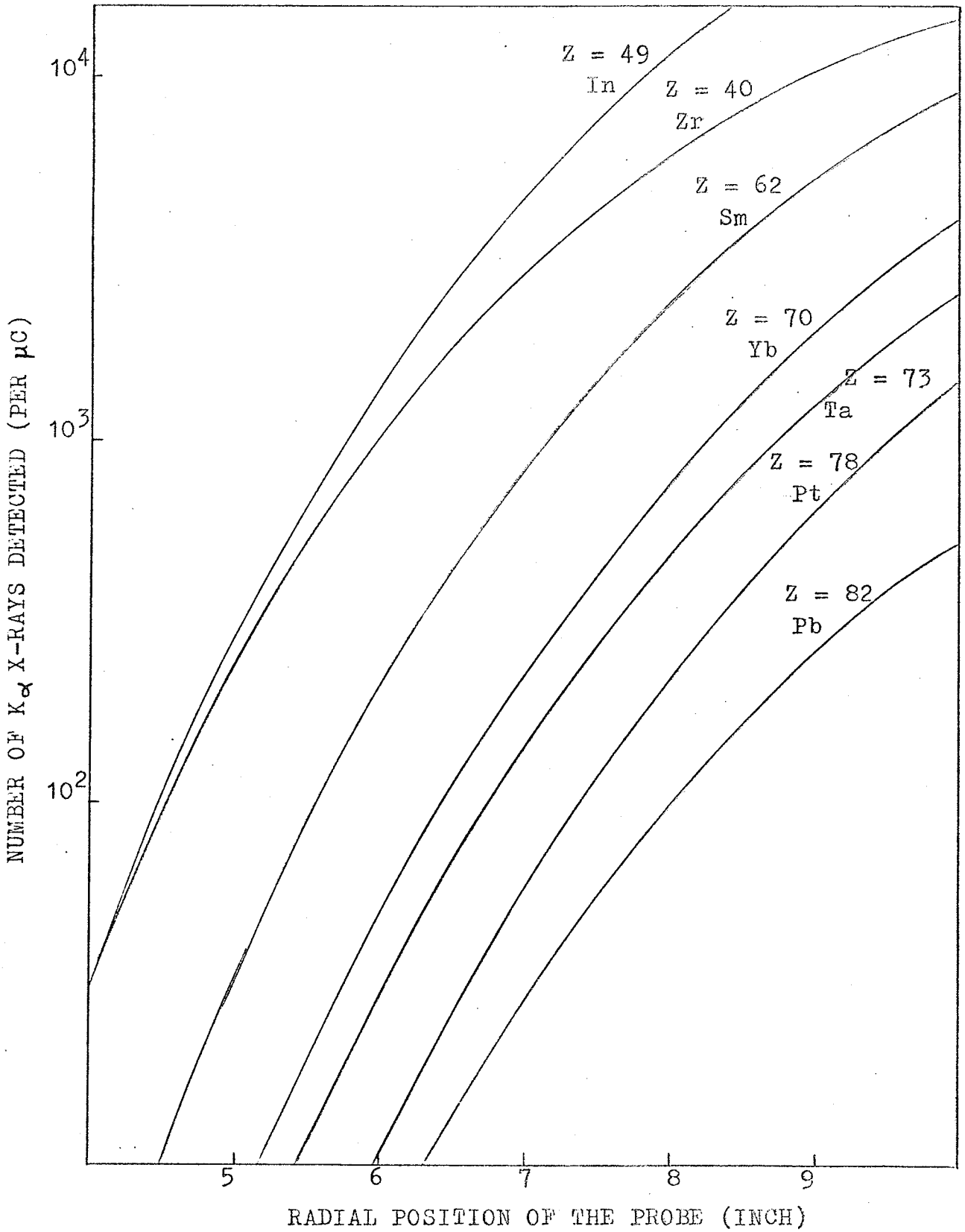

Fig. 2.6 A plot of the number of K X-rays detected per μC of charge vs the position of the probe inside the cyclotron for a set of metals.

some connections inside the machine are silver plated and Ag characteristic X-rays are always present in the spectra obtained.

It is important to note that the curves plotted in Figure 2.6 are not "absolute". They are only valid in the configuration of experimental set-up in which the experiment was conducted at the University of Manitoba Cyclotron Laboratory and for the thicknesses of the different metal strips used.

2.3.3 Accuracy of calculation

The number from Figure 2.6 can be readily used to determine the incident current on the different metal strips. Consider for example the spectrum shown in Figure 2.7 which was obtained with the probe located at a radius of 9". The peaks of indium, samarium, ytterbium, tantalum and platinum are observed. As mentioned before, the silver peaks are due to silver plated connection inside the accelerator and the unidentified peaks are associated with low level impurities in the metal strips. The number of detected X-rays per second corresponding to each peak is given in Table 2.4.

It is worth mentioning that the spectra obtained show satellite peaks associated with main peaks due to (p, xn) reactions (Ra76). The satellite peaks shown in Figure 2.7 are the ones of europium K_{α_1} (associated with the samarium peak) and lutetium K_{α_1} (associated with the ytterbium peak). The K_{α_2} satellite peaks of Eu and Lu are obscured by the K_{α_1} peaks of Sm and Yt respectively. The K_{β_1} satellite peaks are also obscured by the K_{β_2} of Sm and Yt while the K_{β_2} satellite peaks are

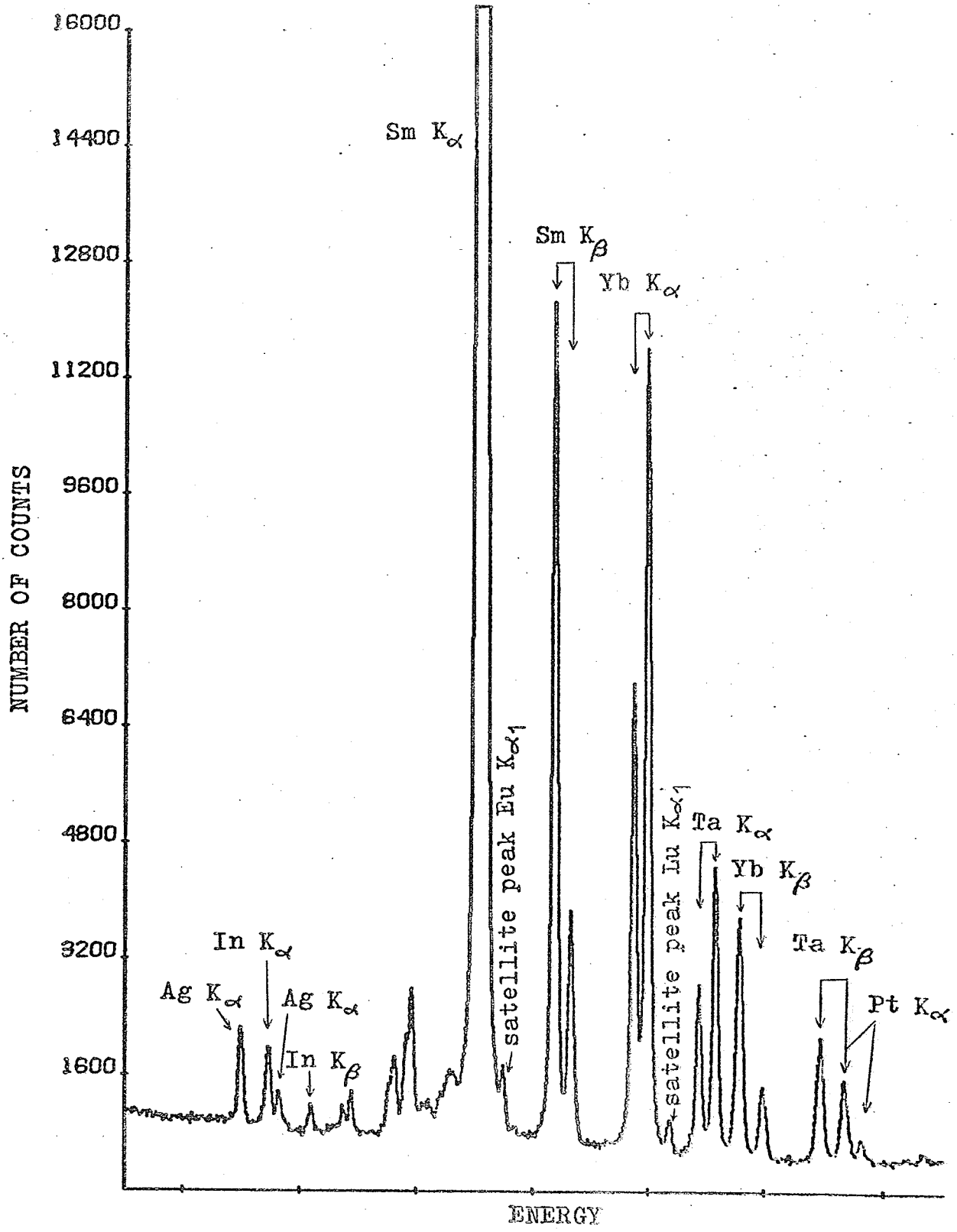

Fig. 2.7 Typical spectrum obtained with the multi-strip probe.

TABLE 2.4

Number of counts (area) of the peaks observed in the spectrum obtained with the probe positioned at a radius of 9" and counting rate associated with them. The spectrum is shown in figure 2.7.

Peak	Area	Counting rate (s^{-1})
In K_α	8830±660	15.8±1.2
In K_β	1613±260	3.9±0.6
Sm K_α	317100±1700	568.0±3.0
Sm K_β	89200±1200	159.8±2.1
Yb K_α	121200±1350	217.1±2.4
Yb K_β	35300±800	63.2±1.5
Ta K_α	25600±700	46.0±1.2
Pt K_α	10050±200	18.0±0.4

too small to be observed. The number of counts in the unresolved peaks was estimated from the number of counts in the satellite peaks by estimating the relative K X-ray intensities. The area of the samarium and ytterbium K_α and K_β peaks were then corrected for the unresolved peaks. One should also note that another correction had to be made in the calculation of the area of the K_α peaks of platinum since the K_β peak of tantalum overlaps with the K_α peak of platinum.

From Figure 2.6, the number of counts that would be detected per second for an incident current of 1 μA is obtained and from them one can easily calculate the incident currents as given in Table 2.5.

The numbers presented in Table 2.5 can not, of course, be more accurate than the parameters (atomic weights, densities, mass absorption coefficients ...) that must be supplied for the calculation. Those numbers are known accurately and should not introduce any significant error. The main source of error would then be the fitted curves used to calculate the stopping power and the ionization cross-section.

The stopping power fit covers the range of energy from 1 MeV to 1.2 GeV. The upper limit certainly does not represent a limitation. It is otherwise for the lower limit since at small incident energy of the protons, they may have an energy lower than 1 MeV before they emerge on the other side of the metal strip or they may even stop in the strip. Since the fit is not valid below 1 MeV, the integration in the calculation must stop once the energy of the protons is below 1 MeV. The error introduced in doing this appears to be negligible until a very low incident energy. Figure 2.8 shows a plot of the total number of Sn characteristic X-rays detected vs depth in target for different incident

TABLE 2.5

Current on the metal strips struck by the proton beam when probe is positioned at a radius of 9".

Peak	Counting rate (s^{-1})		Current (nA)
	Measured	Predicted for current = 1μA	
In K_α	15.8±1.2	21 800	0.72±0.06
In K_β	3.9±0.6	7 690	0.51±0.09
Sm K_α	568.0±3.0	5 060	112.2±0.6
Sm K_β	159.8±2.1	1 460	109.4±1.5
Yb K_α	217.1±2.4	1 960	110.7±1.2
Yb K_β	63.2±1.5	570	110.8±0.9
Ta K_α	46.0±1.2	1 210	38.0±1.0
Pt K_α	18.0±1.2	617	29.2±0.6

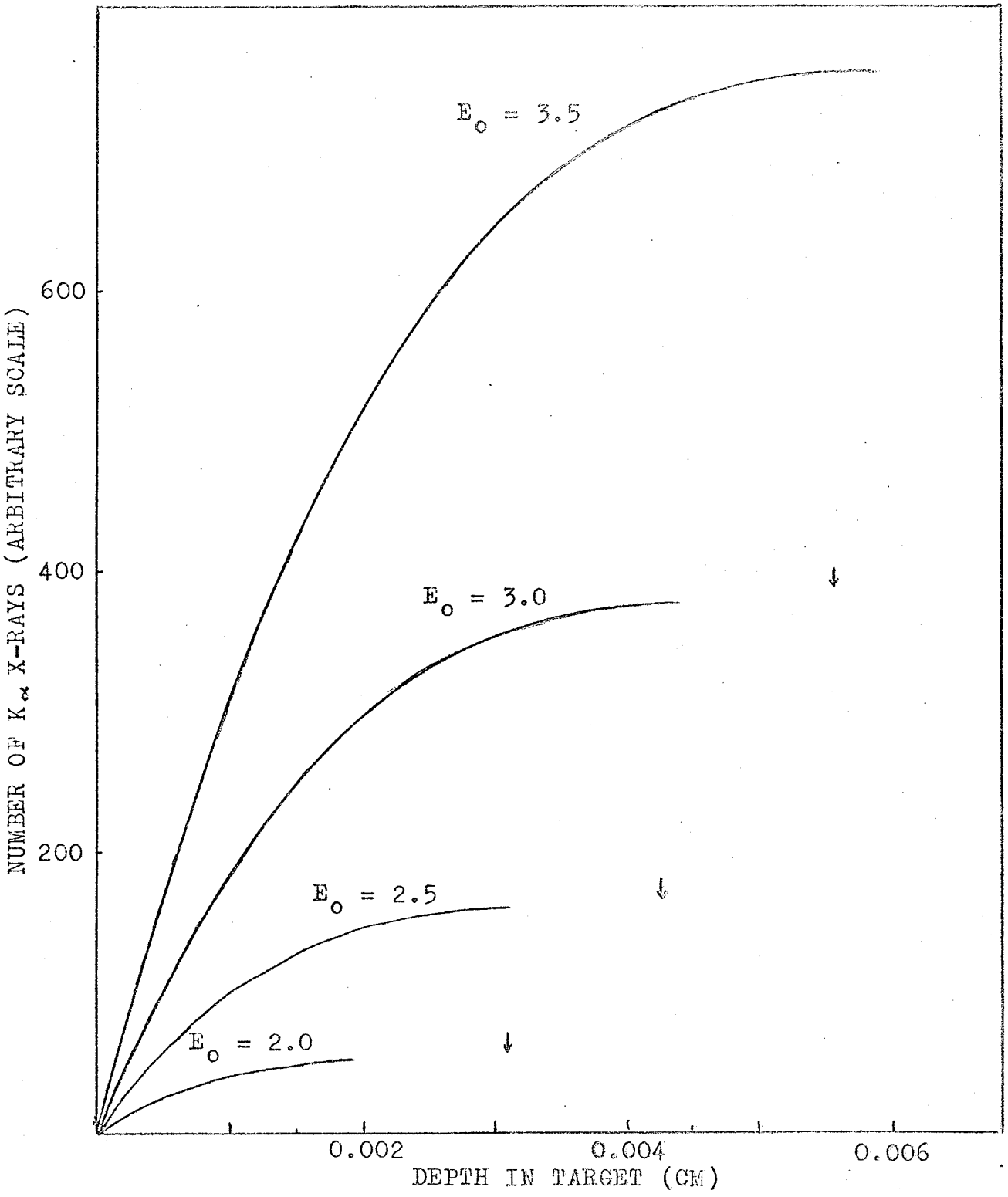

Fig. 2.8 A plot of the number of Sn K_α X-rays detected as a function of depth in target for different incident energies E_o of the protons (in MeV). The curves stop where the energy of the protons goes below 1 MeV. The arrows show the range of the protons.

proton energies (2.0, 2.5, 3.0 and 3.5 MeV). The curves stop at the point where the proton energy drops below 1 MeV. It can be seen from the slope of the curves when the integration stopped that the contribution to the total number of detected X-rays would be negligible from the rest of the path (up to the arrows which show where the protons will stop). This can be easily understood since the K shell ionization cross-section drops drastically at very low energy for the protons (see Figure 2.5).

This approximation then appears to be quite justifiable down to an incident energy of 2 MeV. For radii such that the energy of the proton is still below 2 MeV, the sensitivity of most elements becomes too small and the probe will be of no use anyway.

The quality of the fit in the range of validity (1 MeV to 1.2 GeV) must be evaluated over the two different ranges for which one has a different sets of coefficients. The first set covers the range from 1 MeV to 8 MeV. The stopping power values computed using equation (4) were compared by Barkas and Berger with compilation of experimental values. They claim that the agreement was generally close (remember that it is not the stopping power values that were fitted to experimental measurements but the ranges), although occasional discrepancies up to 4 percent occur which were not incompatible with the experimental errors. For the second set of coefficients covering the range from 8 MeV to 1.2 GeV, the root mean square percentage error was only 1.3 percent. The fit is then excellent.

Consider now the quality of the fit of the K shell ionization

cross-section made by Johansson and Johansson. They affirm that for E/u values between 62 and 1700 the fit is better than 1% and better than 5% down to 18 and up to 3600. Here, the quality of the fit does not depend only on the energy of the protons but also on the K shell ionization energy u of the atom under consideration. Let us consider the two limiting cases of yttrium (Z = 39) and erbium (Z = 68) for which we respectively have u = 17.04 keV and u = 57.48 keV. We then have:

	better than 1%	better than 5%
Yttrium	$1.06 < E < 29.0$	$0.31 < E < 61.3$
Erbium	$3.56 < E < 97.7$	$1.03 < E < 207$

where E is in MeV. The choice of erbium as the element with the highest value of Z that may be used appears here since for an element with a higher value of Z, the fit would not be satisfactory (within 5%) down to a proton energy of 1 MeV at which the integration in equation (2) must stop.

2.4 DETECTION LIMIT

There is always an intrinsic interest in the ultimate capability of an analytical tool with regard to the lowest detectable amount. The detection limit of the probe (understood as the minimum current that can be detected) depends on the number of K X-rays detected and on the statistical uncertainty in the background. Experiments have shown that the background goes up at a rate of roughly 0.5 count per channel per second. This figure is representative of the background when the probe is at a small radius (low incident energy of protons). At higher radii the background is greater (by, say, a factor of 2) but the ionization cross-section of the metals is much higher due to the higher energy of the incident protons. A peak being about 40 channels wide on the scale we use, this means that the background under the peak goes up to 20 counts per second (at low X-ray energy, the background goes up faster but the peaks are also narrower).

In order to get reasonable statistics in a reasonable time (which should not be more than half an hour, which means 360 000 counts in the background under a peak) we should then get a minimum of 1800 counts in the peak (3 times the square root of the background under the peak for which the confidence level is better than 99%) or 1 count per second. Looking at Figure 2.6, one can see that at very small radius (around 5 inches) this means a detection limit of the order of 1 uA for an element like erbium (it would be as high as 10 uA for lead) but only 10 nA for tin. At a radius of 9 inches, the detection limit is less than 1 nA for erbium and less than one tenth of a nA for tin. This large variation in sensitivity shows that as much as possible, the chosen metal should be around tin.

2.5 EXPERIMENTAL CHECK OF THE PROGRAM

Because of the relative complexity of the program used in calculating the intensity of the incident current on the probe, it appeared important to find a way of checking the accuracy of the calculation made using the program. In other words, how can we test the validity of the values of probe current that we obtained from a rather complex and laborious calculation?

The first method uses a stripping foil which is set at a given radius and measures the total current in the beam (in fact, it measures twice the beam current). One then moves the multi-strip probe in until it intercepts the beam (the current on stripping foil drops suddenly to zero). One removes the stripping foil and obtains an X-ray spectrum from which we calculate the total current on the probe. The values of total current obtained in both ways appeared to be in very good agreement taking into account the variations in beam intensity (the average intensity during the measurement can not be assumed to be exactly equal to the beam intensity on the stripping foil just before the measurement).

The second method allows a better accuracy in measurement. A 23 MeV proton beam is extracted from the cyclotron and taken down the "C" line. A thick (0.127 mm) erbium target is then exposed to the beam and the characteristic X-rays induced were collected. Correction was made for the attenuation of the beam within the target so as to evaluate, from the charge collected in the Faraday Cup, the exact charge that hit the erbium target. The experiment was done at three different angles of the incident beam (30, 45 and 60 degrees) and repeated three

times to check repeatability of the measurement. The results of the measurement are presented in Table 2.6. The error associated with each measured value is estimated from the dispersion on the three measurements, while the error associated with the calculated values is estimated by assuming an uncertainty of 0.2 MeV on the energy of the proton beam and 2 degrees in the incident angle of the beam. As can be seen, the agreement is excellent and shows the reliability of the calculation.

TABLE 2.6

Comparison between the total number of characteristic K X-rays detected per μC of charge incident on a thick erbium target as measured experimentally and as calculated using the program "PROBE".

Angle		Number of K X-rays detected per μC	
		MEASURED	CALCULATED
30°	K_α	8 930±110	8 850±475
	K_β	2 640± 90	2 670±115
45°	K_α	12 490±320	12 340±620
	K_β	3 535± 80	3 590±145
60°	K_α	19 680±920	18 140±1100
	K_β	5 530±280	5 180±230

2.6 RESULTS OF MEASUREMENT AND CONCLUSION

A series of measurements using the multi-strip probe was conducted at the University of Manitoba Cyclotron. X-ray spectra were taken with the probe positioned at different radii from 3 up to 9 inches from the center of the machine. Areas of the characteristic peaks were calculated and the current on each metal strip deduced. The vertical distribution of the beam current at different radii is shown in Figure 2.9 in the form of histograms.

The multi-strip probe works well and has a high sensitivity. By moving the probe position in a regular fashion, vertical movement of the beam can be determined, and variation in intensity distribution reliably deduced. Measurements can then be made on an orbit by orbit basis and this feature makes the device invaluable as a diagnostic tool for accelerator studies.

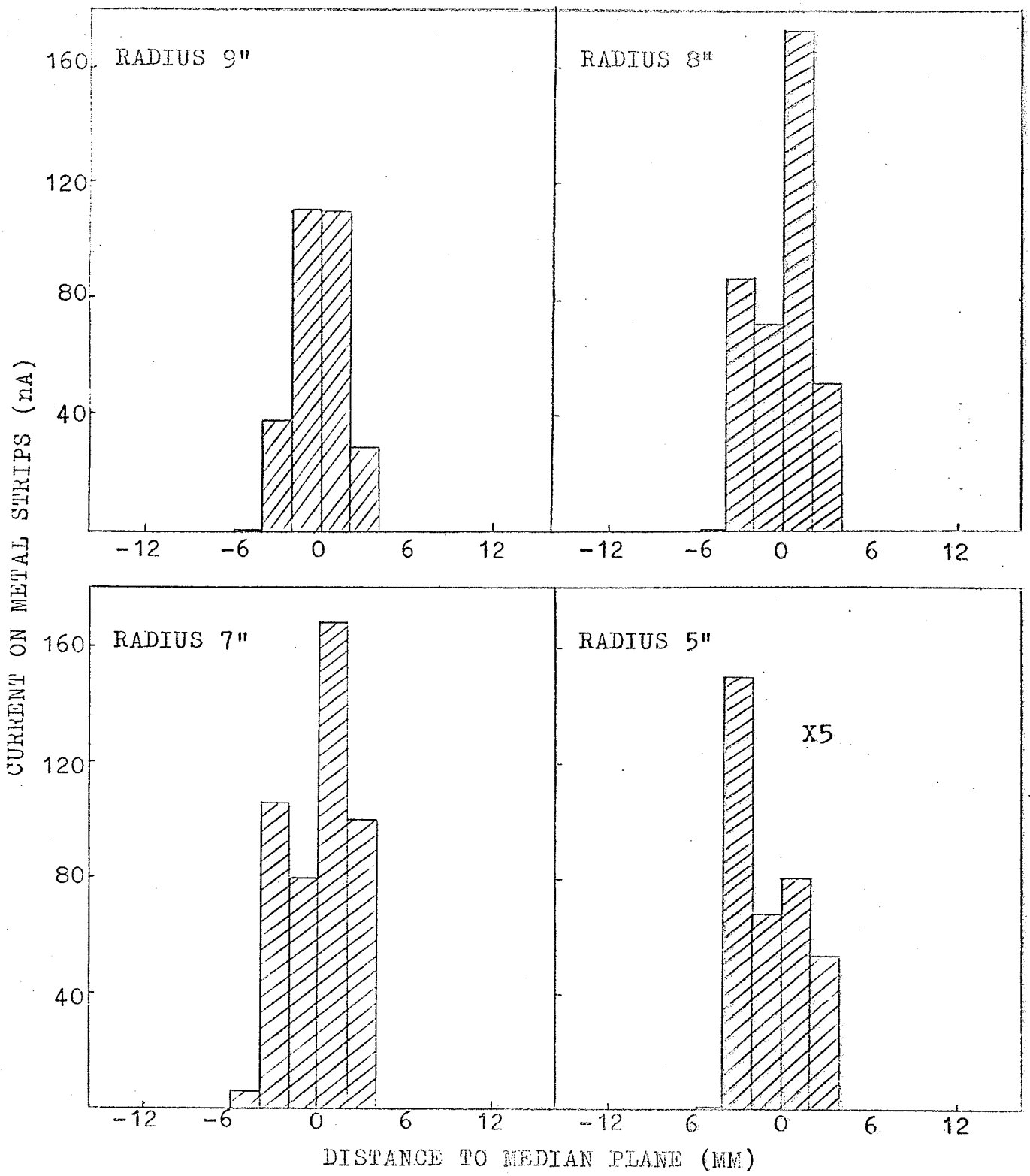

Fig. 2.9 Examples of vertical distribution of current in proton beam at different radii inside the University of Manitoba Cyclotron as deduced using the multi-strip probe.

CHAPTER 3

ANALYSIS OF CESIUM IN MOUSE BRAIN SAMPLES USING THE PIXE TECHNIQUE

3.1 INTRODUCTION

The Department of Pharmacology and Therapeutics of the Faculty of Medicine at the University of Manitoba has been studying the biological effects of cesium ions, to anticipate the possible biohazards. This work, started by Dr. C. Pinsky, was carried out on mice which were treated for several days (4-7) with daily intraperitoneal injections of cesium chloride (CsCl) at 5.0 mEq/kg. Following this treatment, the mice showed noticeable changes in behaviour and it was felt that these changes could be related to accumulation of cesium in the mouse brain.

The PIXE technique was chosen for making accurate estimations of cesium concentration in the mouse brain samples. Due to the presence of the biologically important alkali earth ions, sodium and potassium, this technique is almost uniquely suited for the detection of cesium in body tissue. These elements often interfere with the chemical estimation (or even detection) of small amounts of cesium in tissue sample; with the PIXE technique, however, they are of no consequence. This is by virtue of the wide energy separation between the K X-rays of cesium (X-ray energies of 30.6, 31.0, 35.0 and 35.8 keV) and the other alkali metals (with energies of less than 4 keV).

The proton energy range of the University of Manitoba Cyclotron is perfectly suited for the analysis of cesium by this method. The K shell ionization cross-section of cesium reaches its maximum at an energy of the incident protons of 66 MeV. The energy chosen to carry out the experiment was 30 MeV since at that energy the K shell ionization

cross-section is still fairly high (43.2 barns as compared to 59.9 barns at 66 MeV) and increases only slowly up to the optimum energy.

A large part of the background in the K X-ray fluorescence spectra can be attributed to secondary electron bremsstrahlung. The reason for this assumption is the fact that the background spectrum decreases rapidly up to an X-ray energy of $E_x = 4mE/M$ which is the maximum energy transfer from a projectile of mass M and energy E to a free electron of mass m. The somewhat lower proton energy of 30 MeV, which while having a lower ionization cross-section, has the advantage of a lower bremsstrahlung background, appeared to be a good compromise.

3.2 TECHNIQUE OF MEASURING CESIUM CONCENTRATION IN SAMPLES

3.2.1 Preparation of target samples

The technique used to estimate the concentration of cesium in mouse brain samples employs an internal standard, namely dysprosium, which, being a member of the lanthanide series (rare earth), is not naturally present in the mouse brain or any other body tissue. The concentration of dysprosium in the samples is exactly known and it will be seen later on how the concentration of cesium can be worked out from there.

The samples are prepared in the following way. A precisely known amount of a dysprosium salt (dysprosium chloride hexahydrate, $DyCl_3.6H_2O$) is dissolved in distilled water as to give a concentration of dysprosium of the order of 1500 PPM (or 1.5 mg of Dy per g of solution). The brain sample (of known weight W_b) is added to a 0.7 ml solution of the dopant and is homogenized by 20 seconds maceration in a Polytron homogenizer. The problem is now reduced to calculating the concentration of cesium in the homogenate as compared with the concentration of dysprosium. From there it is straightforward to calculate the total amount of cesium present in the homogenate and, since all of the cesium present in it originates from the brain sample, the ratio weight of cesium to weight of the brain will lead to the average concentration of cesium in the sample.

3.2.2 Experimental technique and theoretical estimation

The target sample is prepared by depositing a small amount (about 20 µg) of homogenate on a precleaned mylar (*) film (480 µg/cm^2) cemented over an oval aperture on an aluminum target holder. The target is then allowed to dry under a heat source. The target holder (and target) is fixed on the target ladder which is mounted on top of the "PIXE cube" located on the "C" line (see Figure 3.1). Up to twelve targets can be mounted simultaneously on the ladder. The target is exposed to approximately 7.5 µC of a 30 MeV proton beam (5 nA, 20 to 30 minutes). The characteristic X-rays of both cesium and dysprosium leave the PIXE cube through a 1 mil thick Kapton window, are detected by means of an Ortec (Model 1113-10205) hyperpure germanium detector, recorded using the data collection program Mirad in a 1024 channels spectrum and stored on DEC tape for off-line analysis (see Figure 3.2). Figure 3.3 shows a typical spectrum obtained by this method. The K_α and K_β X-ray peaks of both elements are well separated and this allows easy counting of the number of characteristic X-rays detected in each peak. Knowing the relative intensity of the cesium and dysprosium K X-ray peaks is, of course, essential to the calculation of the amount of cesium present in the homogenate.

---

* Polyester film, Registered TM DUPONT.

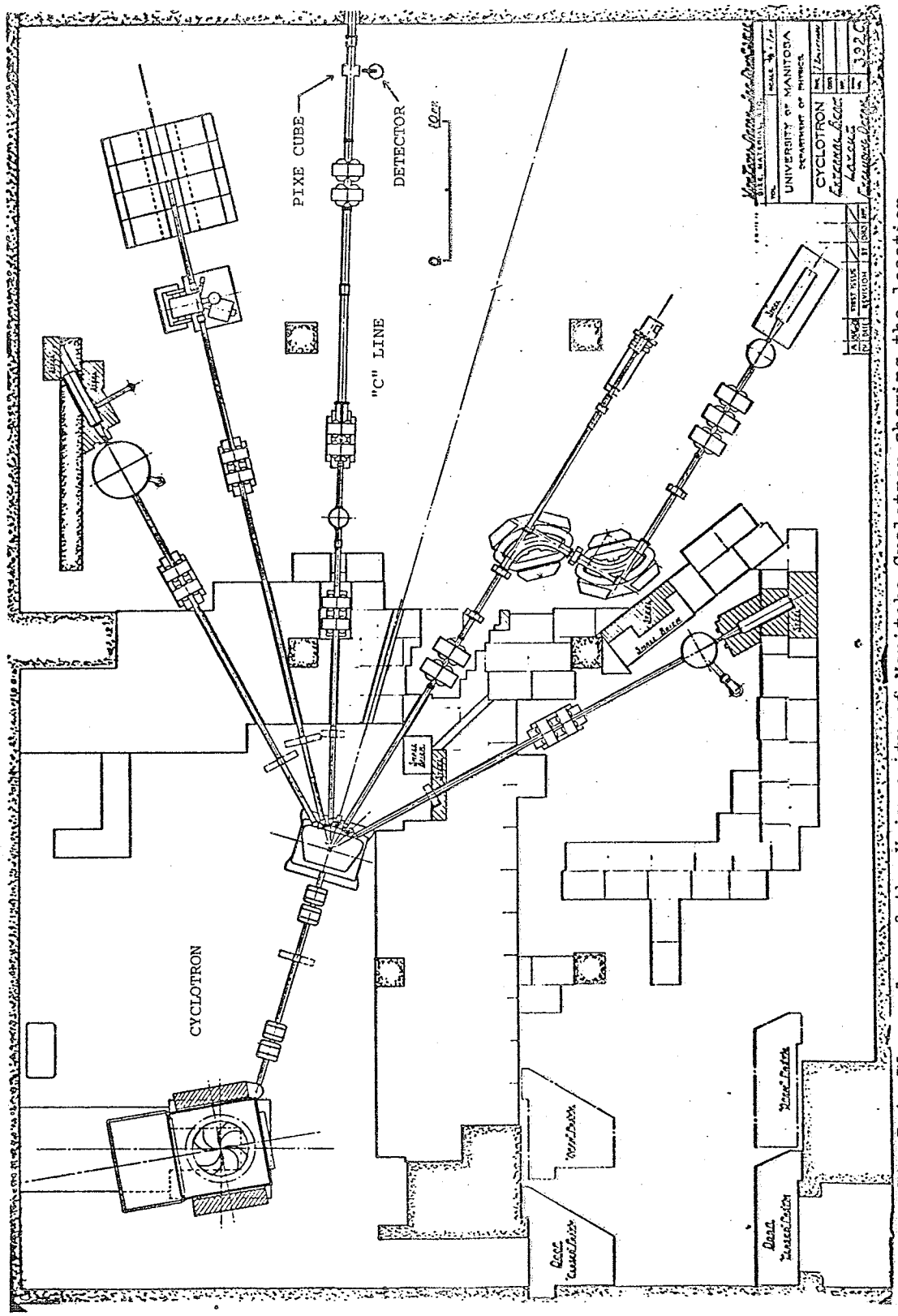

Fig 3.1 Floor plan of the University of Manitoba Cyclotron showing the location of the "PIXE cube" on "C" line.

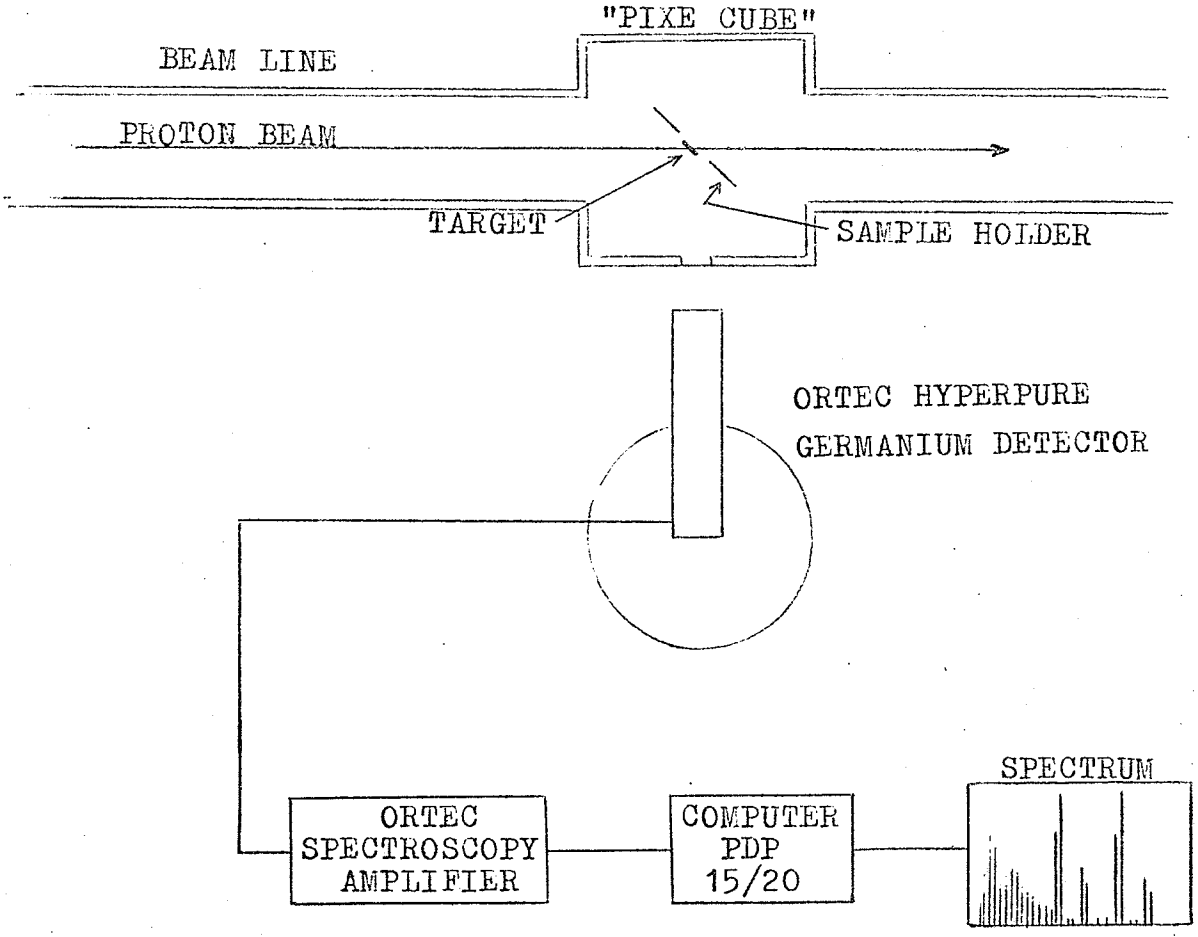

Fig. 3.2 Diagram of experimental set-up in PIXE experiments.

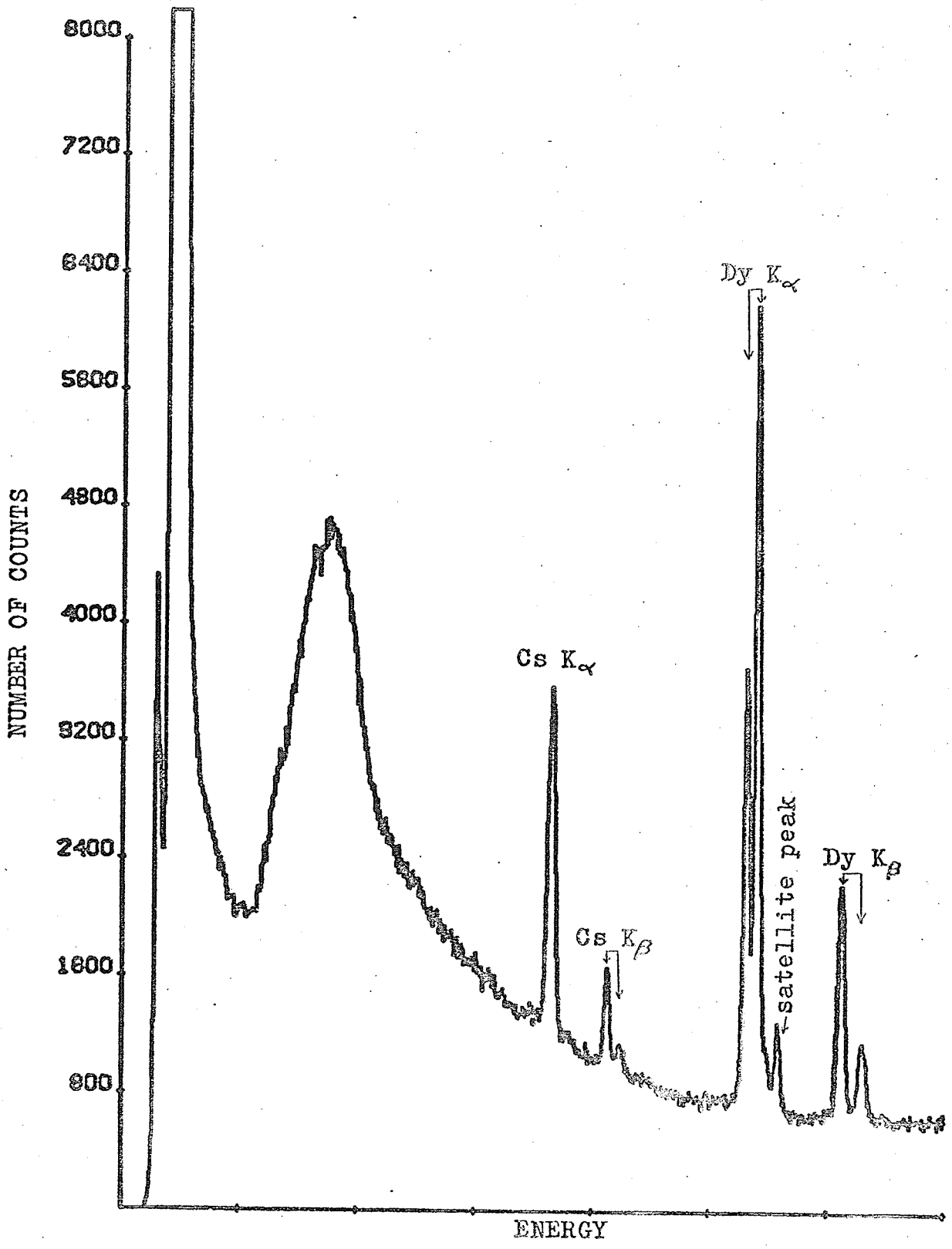

Fig. 3.3 Typical X-ray spectrum of mouse brain sample.

It should be mentioned that the spectrum in Figure 3.3 shows a satellite peak associated with the K_α peak of dysprosium. It corresponds to the K_{α_1} peak of holmium. The K_{α_2} peak is obscured by the K_{α_1} peak of dysprosium and correction must be made for it in the calculation of the area of the peak of dysprosium.

The calculation of the concentration of cesium in a brain sample requires the knowledge of the "K X-ray Production Cross-Section" which is a measure of the probability that a given atom exposed to a proton beam will emit a K X-ray. As mentioned before, the PIXE experiments made with brain samples used 30 MeV protons. The X-ray production cross-section of the K_α and K_β peaks of both cesium and dysprosium for an incident energy of 30 MeV are given in Table 3.1. Those numbers were obtained from the semi-empirical formula of Johansson and Johansson (Jo76). Note that the K shell ionization cross-section (not the K X-ray production cross-section) is obtained from the formula. The X-ray production cross-section is obtained by multiplying the K shell ionization cross-section by the fluorescence yield (0.892 for cesium and 0.937 for dysprosium (La79)) which takes into account the fact that the de-excitation process by emission of X-rays is in competition with Auger electron emission. The X-ray production cross-section for each of the K_α and K_β peaks is then obtained from the ratio K_α/K_β (0.235 for Cs and 0.257 for Dy, (Sa74)).

If the X-ray production cross-section is a measure of the probability that an atom will emit an X-ray, the total number of characteristic X-rays emitted by the target will also depend on the total number of atoms in the target and on the intensity of the proton beam (number of protons per cm^2 per second).

TABLE 3.1

K X-ray production cross-sections (in barns) of cesium and dysprosium for an energy of the incident protons of 30 MeV.

	Cs	Dy
K_α	31.3±0.4	9.34±0.16
K_β	7.35±0.10	2.40±0.04

Assume for the time being that the number of cesium atoms in the target, N(Cs), is the same as the number of dysprosium atoms, N(Dy). Since the two types of atoms are exposed to the same beam, the ratio of the number of cesium K_α X-rays to the number of dysprosium K_α X-rays emerging from the target will be

$$\frac{\sigma\ (Cs\text{-}\alpha)}{\sigma\ (Dy\text{-}\alpha)} = \frac{31.3 \text{ barns}}{9.34 \text{ barns}} = 3.35.$$

Any departure from this ratio will mean a departure from the ratio 1:1 in the number of cesium and dysprosium atoms present in the target. This is done assuming that X-ray attenuation in target can be neglected. This assumption appears to be quite justifiable since the targets used are thin (a few tens of μg per cm^2) and the energies of the K X-rays of cesium and dysprosium are relatively high.

The number of cesium atoms in the target is obtained from the relation

$$N(Cs) = N(Dy)\ \frac{Ct(Cs\text{-}\alpha)}{Ct(Dy\text{-}\alpha)}\ \frac{\sigma(Dy\text{-}\alpha)}{\sigma(Cs\text{-}\alpha)}, \qquad \text{Eq. (1)}$$

where Ct(Cs-α) and Ct(Dy-α) are respectively the numbers of counts under the K_α peaks of cesium and dysprosium. In this example, we use the K_α peaks of cesium and dysprosium, but any of the four combinations of K_α or K_β peaks would yield the same result.

3.2.3 Correction for attenuation and detector efficiency

Unfortunately, the situation is not as simple as this. When

protons hit the target, a small but significant fraction of the protons are "elastically scattered" from target nuclei and reach the detector. In order to protect the detector from those protons, 2.0 cm of paraffin, is inserted between the target and the detector. This is enough to stop 33 MeV protons while allowing most X-rays to pass through. The transmission of the paraffin being a function of X-ray energy, the ratio of the K_α X-rays of cesium and dysprosium reaching the detector will not be the same as the ratio of X-rays leaving the target.

The transmission of X-rays through 2.0 cm of paraffin ($(CH_2)_n$) was calculated using the total attenuation cross-section of carbon and hydrogen (Ve73). If μ_1 and μ_2 are the total attenuation cross-section of respectively carbon and hydrogen (which are a function of X-ray energy), the transmission through the absorber is

$$T = \exp(-\mu_1 X_1 - \mu_2 X_2), \qquad \text{Eq. (2)}$$

where X_1 and X_2 are the thicknesses of the absorber for carbon (1.599 g/cm^2) and hydrogen (0.266 g/cm^2). The calculation leads to the numbers presented in Table 3.2.

In order to check the calculation, the attenuation of the absorber was also calculated for the gamma-ray and X-ray peaks from an americium 241 source producing gamma-rays of 59.57 keV and 26.35 keV energy and X-rays at 20.77, 17.74, 16.84 and 13.94 keV, and compared with an experimental measurement. Two spectra from Am-241 were obtained using a germanium detector and a radioactive source kept at a constant distance

TABLE 3.2

Transmission of K X-rays of cesium and dysprosium through 2 cm of paraffin. The numbers are a weighted average of the transmission for the two energies associated to the K_α and K_β.

	Cs	Dy
K_α	0.607	0.666
K_β	0.632	0.680

from the source. One spectrum was obtained without the absorber and another with the absorber. The ratio of the areas under the corresponding peaks (after normalization) then lead to the transmission. It can be seen from the results in Table 3.3 that the agreement between calculated and measured values is excellent.

It should also be mentioned that this paraffin absorber presents the advantage of attenuating considerably the low energy part of the bremsstrahlung background so reducing the counting rate for undesirable low energy X-rays.

Detector efficiency must also be taken into account since it varies with X-ray energy. It decreases for low energy X-rays (below 30 keV) because of attenuation in the thin beryllium window in front of the detector sensitive volume and in the dead layer of the germanium crystal. Efficiency also decreases for high energy X-rays (above 60 keV) because of the limited thickness of the germanium crystal. But in the energy region of the Cs and Dy K X-rays, (between 30 and 54 keV) the efficiency of the detector is practically 100% and no correction has to be made for it. Equation (1) can then be written

$$N(Cs) = N(Dy) \frac{Ct(Cs-\alpha)}{Ct(Dy-\alpha)} \frac{\sigma(Dy-\alpha)}{\sigma(Cs-\alpha)} \frac{T(Dy-\alpha)}{T(Cs-\alpha)} \qquad \text{Eq. (3)}$$

3.2.4 Concentration of cesium in brain samples

The amount of cesium and dysprosium present in a target is obtained from the number of atoms present knowing the atomic weight of

TABLE 3.3

Comparison between the calculated values of transmission for γ-rays and X-rays of Am-241 through 2.00±0.01 cm of paraffin and the experimentally measured values. The statistical error associated with the experimental values corresponds to one standard deviation.

E (keV)	T (cal)	T (meas)
13.945	0.199±0.002	0.217±0.006
16.837	0.338±0.002	0.335±0.017
17.740	0.374±0.002	0.377±0.008
20.774	0.468±0.002	0.504±0.024
26.35	0.567±0.002	0.583±0.028
59.57	0.692±0.001	0.693±0.005

the elements.

$$W(Cs) = \frac{A(Cs)N(Cs)}{N}, \qquad \text{Eq. (4a)}$$

$$W(Dy) = \frac{A(Dy)\ N(Dy)}{N}, \qquad \text{Eq. (4b)}$$

where A is the atomic weight (132.9 g for cesium and 162.5 g for dysprosium) and N is Avogadro's number (6.023×10^{23} mole^{-1}). Combining equations (4) gives

$$W(Cs) = W(Dy)\ \frac{A(Cs)\ N(Cs)}{A(Dy)\ N(Dy)} \qquad \text{Eq. (5)}$$

Replace N(Cs) by its value in equation (3) to obtain

$$W(Cs) = W(Dy)\ \frac{A(Cs)}{A(Dy)}\ \frac{Ct(Cs-\alpha)}{Ct(Dy-\alpha)}\ \frac{\sigma(Dy-\alpha)}{\sigma(Cs-\alpha)}\ \frac{T(Dy-\alpha)}{T(Cs-\alpha)} \qquad \text{Eq. (6)}$$

W(Cs) and W(Dy) are, by definition, the amounts of cesium and dysprosium present in the target. Since the ratio W(Cs)/W(Dy) is the same in the target as it is in the original homogenate, if one uses in equation (6) W(Dy) as the total amount of dysprosium in the whole homogenate, W(Cs) will also be the total amount of cesium present in the homogenate. Since all of the cesium comes from the brain sample, division of W(Cs) by the weight of the brain sample W_b gives the concentration of cesium in the sample

$$[Cs] \text{ in PPM} = \frac{W(Cs) \text{ in } \mu g.}{W_b \text{ in g}} \qquad \text{Eq. (7)}$$

Using equation (6) we then have

$$[Cs] = \frac{W(Dy)}{W_b} \frac{Ct(Cs\text{-}i)}{Ct(Dy\text{-}j)} C(Cs\text{-}i, Dy\text{-}j), \qquad \text{Eq. (8a)}$$

where

$$C(Cs\text{-}i, Dy\text{-}j) = \frac{A(Cs)\,\sigma(Dy\text{-}j)\,T(Dy\text{-}j)}{A(Dy)\,\sigma(Cs\text{-}i)\,T(Cs\text{-}i)} \qquad \text{Eq. (8b)}$$

with

$$i, j = \alpha \text{ or } \beta.$$

σ and T are given in Tables 3.1 and 3.2, and A are the atomic masses. The calculation for the four different combinations leads to the following numbers.

$$C(Cs\text{-}\alpha, Dy\text{-}\alpha) = 0.268$$

$$C(Cs\text{-}\beta, Dy\text{-}\alpha) = 1.10$$

$$C(Cs\text{-}\alpha, Dy\text{-}\beta) = 0.069$$

$$C(Cs\text{-}\beta, Dy\text{-}\beta) = 0.288$$

with a possible error of 2% due mainly to the uncertainty in the fluorescence yield and in the ionization cross-section. It is important to note that the calculation of [Cs] does not require the knowledge of the amount of solution deposited on target or hit by the beam. This is particularly important since the beam spot may very well be inhomogeneous or may hit only a part of the target.

3.3 CONCLUSION

The PIXE technique is now working well and is used in routine analysis of brain samples. The K X-ray fluorescence spectra of large numbers of samples (up to 30) have been obtained within one day. The analysis of the spectra (estimation of areas of the K X-ray peaks of cesium and dysprosium) is performed on PDP 15/40 computer using a peak fitting program called COAXS. From those areas, cesium concentration in mouse brain can be reliably deduced using equation (9).

Detection limit of a few PPM of cesium (2 to 20) are currently obtained and this appears to be largely sufficient since the cesium concentration generally observed is in the range 100 to 1000 PPM.

3.4 FUTURE WORK

With the actual technique, trace element concentration can be measured accurately down to a few PPM as long as internal dopant can be used. Unfortunately this is not always the case (eg. when we want to measure trace element concentration in a single human hair). It then becomes necessary to be able to measure the absolute mass of the elements present. This can be done in the following way. The number of detected characteristic K X-rays of a given element present in a target exposed to a proton beam is given by

$$X = \frac{\Omega\sigma N\varepsilon T}{Ae} \int_S \rho\rho' \, dS, \qquad \text{Eq. (9)}$$

where

Ω is the solid angle subtended by the detector,

σ is the K X-ray production cross-section,

N is Avogadro's number,

A is the atomic mass,

e is the proton charge,

ε is the detector efficiency,

T is the transmission through the paraffin attenuator,

ρ is the areal density of the element under consideration in the target (g/cm^2) which may vary within the target,

ρ' is the areal density of charge of the incident beam (C/cm^2), which may also vary over the target.

The integration is performed over the area of the beam spot S. If it is possible to obtain a uniform beam spot (ρ' = constant = Q/S where Q is the total charge collected in the Faraday Cup and S is the cross-sectional area of the beam) then equation (9) reduces to

$$X = \frac{\Omega\sigma N\varepsilon Q}{AeS} \int_S \rho \, dS \qquad \text{Eq. (10)}$$

and the integration is equal to the absolute amount of the element under consideration present in the target (M) assuming that the beam covers the whole sample. Since the number X is known from the experimental measurement, rearrangement of the last equation gives

$$M = \frac{AeSX}{\Omega \sigma N \varepsilon Q} \qquad \text{Eq. (11)}$$

Knowing the mass of the sample exposed to the beam, one can easily work out the concentration directly from the mass M without the use of an internal dopant.

It is possible to measure the absolute mass of a given element present in the target, but the homogeneity of the beam imposes a rather severe restriction. The method that has been developed at the University of Manitoba cyclotron to obtain a uniform spot uses a steering magnet located about 10 m before the PIXE cube to repeatly scan a very small beam spot across the target along two axes. For this purpose, two specially designed power supplies were built so to generate a triangular wave form for the current in the steering magnet. At the intensity of

of magnetic field that one needs, the induced magnetic field varies linearly with the current and a uniform scan of the target by the beam spot is obtained. The first tests will start in the coming months.

REFERENCES

(Ba64) W.H. Barkas and M.J. Berger, Tables of Energy Losses and Ranges of Heavy Charged Particles, Studies in Penetration of Charged Particles in Matter, Nuclear Science Series, Report Number 39, National Academy of Sciences-National Research Council, Publication 1133.

(Ba72) W. Bambinek, Proc. Int. Conf. on Inner Shell Ionization Phenomena (1972), eds. R.F. Fink, S.T. Manson, J.M. Palms and P.V. Rao (US Atomic Energy Commission CONF-729404, 1973)

(Be70) E.P. Bertin, Principles and Practice of X-ray Spectrometric Analysis, Plenum Press, 1970.

(De75) G. Deconnick, G. Demortier and F. Bodart, Application of X-ray Production by Charged Particles to Elemental Analysis, Atomic Energy Review, Vol. 13 (1975) 367.

(Jo76) Sven A.E. Johansson and Thomas B. Johansson, Analytical Application of Particles Induced X-Ray Emission, Nuclear Instruments and Methods, 137 (1976) 473.

(La79) A. Lagenberg and J. van Eck, An Evaluation of K-Shell Fluorescence Yields: Observation of Outer-Shell Effects, J. Phys. B. Atom. Molec. Phys., Vol. 12, No. 8, (1979) 1331.

(La80) C. Lapointe and J.S.C. McKee, A K X-ray Fluorescent Multi-Strip Probe for Accelerator Beam Studies, Nuclear Instruments and Methods, 174 (1980) 9.

(Oh79) S. Oh, M. de Jong, J. Birchall, I. Gusdal, A. McIlwain and

J.S.C. McKee, An Investigation into Depolarisation of H Beam During Acceleration Inside the University of Manitoba Cyclotron, Annual Research Report 1978-1979, Cyclotron Laboratory, Department of Physics, University of Manitoba, (1979) 6.

(Ra76) C.P. Randell, J.S.C. McKee and S.F.J. Wilk, The Nature of the K X-Ray Satellite Peak is Determined from the Analysis of Fluorescence Spectra Induced by 20-50 MeV Protons, Journal of Physics G, Nuclear Physics 2 (1976) 69.

(Sa74) S.I. Salem, S.L. Panossian and R.A. Krause, Atomic Data Nucl. Data Tables, 14 (1974) 91.

(Ve73) W.M.J. Veigele, Ionization Cross-Section of Photons, Atomic Data, Vol. 5, No. 1 (1973) 61.

(Wo73) Rolf Woldseth, X-Ray Energy Spectroscopy, Kevex Corporation, 1973.

LIST OF PUBLICATIONS

Elemental Analysis of Environmental Samples and the Production of Radiopharmaceuticals at the University of Manitoba Cyclotron Laboratory, M.S.A.L. Al-Ghazi, M.I. Gusdal, C. Lapointe and J.S.C. McKee, Transactions of CNA Conference, Ottawa, 7, (1979).

An Analysis of Lead, Bromine, Zinc and Sulphur in Airborne Particulate Matter by X-ray Fluorescence Spectroscopy, J.S.C. McKee, C. Lapointe and M.L.H. Wise, Journal of Environmental Science and Health, A15(1), 1-23, (1980).

Determination of Mercury in Fish Samples by Proton Induced K X-ray Emission, Z. Kamal, M.S.A.L. Al-Ghazi, J. Birchall J.J.G. Durocher, C. Lapointe, J.S.C. McKee, N.T. Okumusoglu, W.D. Ramsay and N. Videla, Proceedings of the CNA Conference, Winnipeg, 74, (1980).

Diagnostic Tool for Beam Studies Within a Cyclotron, C. Lapointe and J.S.C. McKee, Proceedings of the CNA Conference, Winnipeg, 6, (1980).

A K X-ray Fluorescent Multi-Strip Probe for Accelerator Beam Studies, C. Lapointe and J.S.C. McKee, Nuclear Instruments and Methods, 174, 9, (1980).